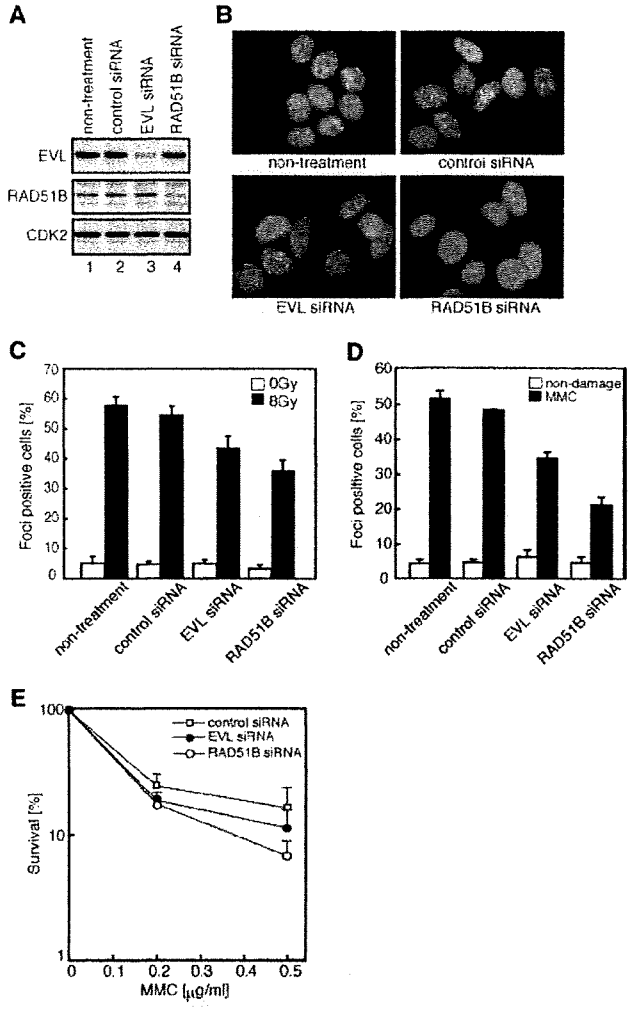

FIGURE 1. **Analyses of the EVL and RAD51B knockdown cells.** *A*, the EVL, RAD51B, and CDK2 proteins in the siRNA-treated MCF7 cells. The *top, middle,* and *bottom panels* indicate the expression levels of the EVL, RAD51B, and CDK2 proteins, respectively. The proteins were detected by Western blotting. *Lanes 1* and *2*, control experiments without siRNA and with a control siRNA, respectively. *Lanes 3* and *4*, experiments with EVL siRNA and RAD51B siRNA, respectively. *B*, RAD51 foci formation. The MCF7 cells were treated with γ-ray irradiation (8 grays). The cells without treatment, with a control siRNA treatment, with an EVL siRNA treatment, or with a RAD51B siRNA treatment are presented. *C*, graphic representation of the RAD51 foci formation after γ-ray irradiation (8 grays). The cells containing more than 10 RAD51 foci were scored as positive and were plotted. The averages of three independent experiments are plotted with S.D. values. *D*, graphic representation of the RAD51 foci formation after MMC treatment. The cells containing more than 10 RAD51 foci were scored as positive and were plotted. The averages of three independent experiments are plotted with S.D. values. *E*, sensitivity to MMC. *Open squares, closed circles,* and *open circles*, experiments with a control siRNA, EVL siRNA, and RAD51B siRNA, respectively. The averages of three independent experiments are plotted with S.D. values.

The cells containing more than ten RAD51 foci after ionizing radiation treatment were scored as positive, because many cells containing fewer than 10 RAD51 foci were observed, even in the absence of DNA damage. The EVL knockdown MCF7 cells exhibited a clear reduction in RAD51 foci formation (Fig. 1, *B* and *C*, and supplemental Fig. 1). Consistent with previous studies (39, 44), the RAD51B knockdown MCF7 cells exhibited a comparable reduction in RAD51 foci formation on the DSB

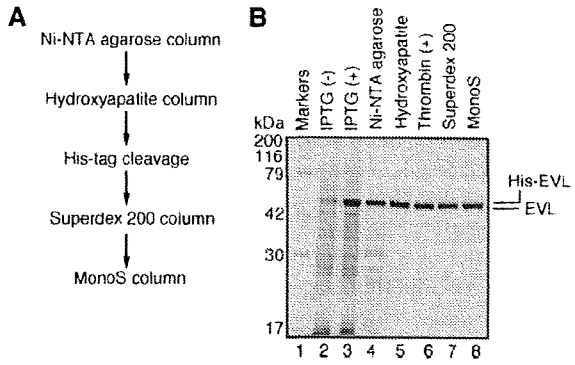

FIGURE 2. **Purification of the human EVL protein.** *A*, schematic representation of the purification steps for the Evl protein. *B*, proteins from each purification step were analyzed by 12% SDS-PAGE with Coomassie Brilliant Blue staining. *Lane 1*, molecular mass markers; *lanes 2* and *3*, whole cell lysates before and after induction with isopropyl-1-thio-β-D-galactopyranoside (*IPTG*), respectively. *Lanes 4–8*, samples from the peak Ni^{2+}-NTA-agarose (Invitrogen) fraction, the peak hydroxyapatite (Bio-Rad) fraction, the fraction after the removal of the hexahistidine tag, the peak Superdex 200 fraction (GE Healthcare), and the peak MonoS fraction (GE Healthcare), respectively.

sites after ionizing radiation (Fig. 1, *B* and *C*). Reduced RAD51 foci formation was also observed in the EVL knockdown cells after treatment with an interstrand cross-linking agent, MMC (Fig. 1*D*). These results suggested that, like the RAD51B protein, the EVL protein functions in RAD51 assembly on DSB sites in the HRR pathway.

On the other hand, the EVL knockdown cells did not exhibit significant increase in sensitivity to MMC (Fig. 1*E*). The weak MMC sensitivity in the EVL knockdown cells, as compared with that in the RAD51B knockdown cells, may be explained by the presence of EVL paralogs, such as the MENA and VASP proteins, which may complement the functions of the EVL protein.

Interaction of the EVL Protein with the RAD51 and RAD51B Proteins—The human EVL protein was purified as a recombinant protein by a five-step procedure (Fig. 2*A*). In this procedure, the His_6 tag was uncoupled with thrombin protease from the EVL portion, which then migrated slightly faster than the His_6-tagged EVL protein upon SDS-polyacrylamide gel electrophoresis (Fig. 2*B*, *lane 6*).

We then tested whether the EVL protein binds to the RAD51 protein, because the EVL knockdown cells exhibited a reduction in RAD51 foci formation (Fig. 1, *B* and *C*). To do so, we prepared Affi-Gel 10 beads chemically conjugated with the EVL protein and performed pulldown assays with HeLa cell extracts. As shown in Fig. 3*A* (*lane 2*), the endogenous RAD51 protein in the HeLa cell extract was detected in the EVL-bound fraction over the background level. Like the RAD51 protein, the endogenous RAD51B protein in the HeLa cell extract was also detected in the EVL-bound fraction (Fig. 3*B*, *lane 2*). These results suggested that the EVL protein binds to the RAD51 and RAD51B proteins.

To verify the EVL binding to the RAD51 and RAD51B proteins, we performed SPR analyses. The RAD51 protein interacted with the EVL-conjugated sensor chip (Fig. 3*C*). The RAD51B protein also significantly interacted with the EVL protein (Fig. 3*D*). In contrast, the DMC1 protein, which shares about 50% amino acid identity with the RAD51 protein, exhib-

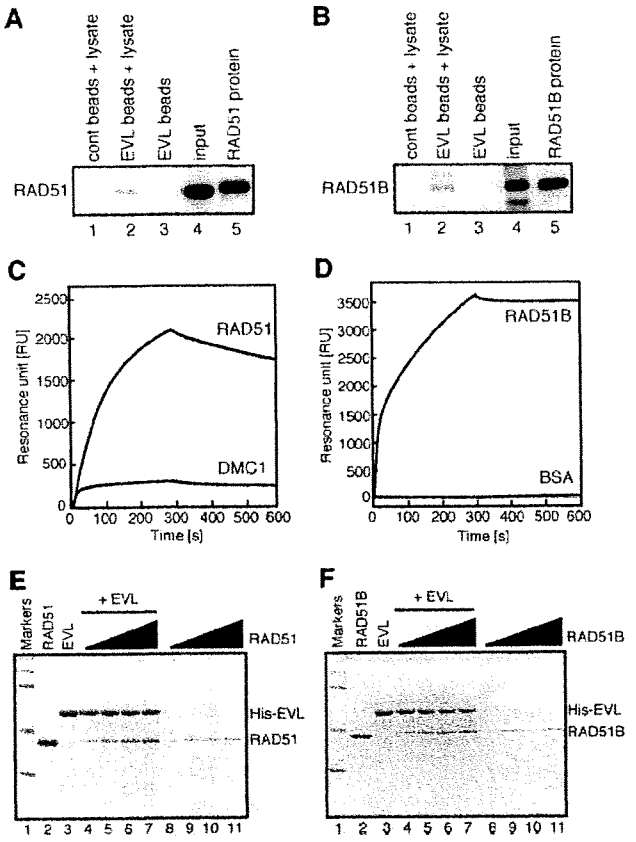

FIGURE 3. **The EVL protein binds to the RAD51 and RAD51B proteins.** *A* and *B*, pulldown assay. Affi-Gel 10 beads chemically conjugated with the EVL protein were incubated with a HeLa whole cell extract. Proteins bound to the EVL beads were separated by SDS-PAGE and were analyzed by Western blotting. *A*, the endogenous RAD51 protein was probed with an anti-RAD51 polyclonal antibody. *Lanes 1* and *2*, experiments with the control Affi-Gel 10 beads and the EVL beads, respectively, in the presence of the HeLa cell lysate. *Lane 3*, a control experiment with the EVL beads in the absence of the HeLa cell lysate. The input HeLa cell lysate (10 μg of protein) and the purified RAD51 (2 ng) protein were applied in *lanes 4* and *5*, respectively. *B*, the endogenous RAD51B protein was probed with an anti-RAD51B polyclonal antibody. *Lanes 1* and *2*, experiments with the control Affi-Gel 10 beads and the EVL beads, respectively, in the presence of the HeLa cell lysate. *Lane 3*, a control experiment with the EVL beads in the absence of the HeLa cell lysate. The input HeLa cell lysate (10 μg) and the purified RAD51B protein (2 ng) were applied in *lanes 4* and *5*, respectively. *C*, surface plasmon resonance analyses of the EVL-RAD51 and EVL-DMC1 interactions. Sensorgrams for RAD51 and DMC1 binding to the immobilized EVL protein are presented. The RAD51 and DMC1 concentrations were 1 μM. *D*, surface plasmon resonance analysis of the EVL-RAD51B interaction. Sensorgrams for RAD51B and BSA binding to the immobilized EVL protein are presented. The RAD51B and BSA concentrations were 1 μM. *E* and *F*, the Ni^{2+}-NTA-agarose pulldown assay with the His_6-tagged EVL and RAD51 (*E*) or RAD51B (*F*) proteins. *Lane 1*, molecular mass markers (200, 116, 79, 42, and 30 kDa). *Lanes 2* and *3*, RAD51 (*E*) or RAD51B (*F*) and the His_6-tagged EVL proteins. *Lanes 4–7* and *lanes 8–11*, experiments in the presence and absence of the His_6-tagged EVL, respectively. The concentration of the His_6-tagged EVL protein was 0.45 μM. The RAD51 or RAD51B concentrations were 0.5 μM (*lanes 4* and *8*), 1 μM (*lanes 5* and *9*), 1.5 μM (*lanes 6* and *10*), and 2 μM (*lanes 7* and *11*).

ited little binding to the EVL protein (Fig. 3C). These results indicated that the EVL protein specifically binds to the RAD51 and RAD51B proteins.

We finally confirmed the EVL binding to the RAD51 and RAD51B proteins by the Ni^{2+}-NTA-agarose pulldown assay. In this assay, the His_6-tagged EVL protein was used as the bait

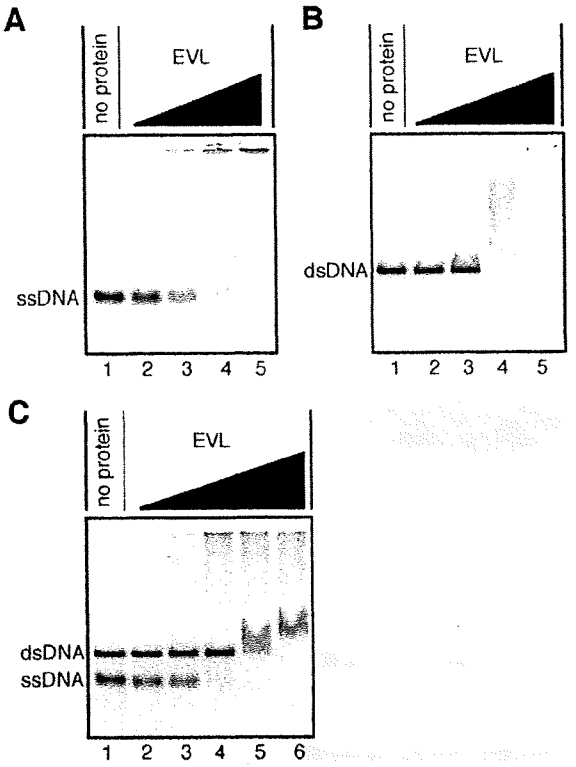

FIGURE 4. **DNA binding activities of the EVL protein.** ϕX174 ssDNA (20 μM) and/or ϕX174 linear dsDNA (20 μM) were each incubated with the EVL protein at 37 °C for 15 min. The samples were then separated by 0.8% agarose gel electrophoresis in TAE buffer and were visualized by ethidium bromide staining. *A*, ssDNA binding. *Lane 1*, a negative control experiment without the EVL protein. The EVL concentrations were 0.1 μM (*lane 2*), 0.2 μM (*lane 3*), 0.4 μM (*lane 4*), and 0.8 μM (*lane 5*). *B*, dsDNA binding. *Lane 1*, a negative control experiment without the EVL protein. The EVL concentrations were 0.1 μM (*lane 2*), 0.2 μM (*lane 3*), 0.4 μM (*lane 4*), and 0.8 μM (*lane 5*). *C*, competitive binding to ssDNA and dsDNA. *Lane 1*, a negative control experiment without the EVL protein. The EVL concentrations were 0.1 μM (*lane 2*), 0.2 μM (*lane 3*), 0.4 μM (*lane 4*), 0.8 μM (*lane 5*), and 1.2 μM (*lane 6*).

protein, since the EVL protein covalently conjugated to the Affi-gel beads did not enter the polyacrylamide gel. Consistently, the purified RAD51 and RAD51B proteins bound to the His_6-tagged EVL protein were captured by the Ni^{2+}-NTA beads in a concentration-dependent manner (Fig. 3, *E* and *F*). In the presence of excess amounts of the RAD51 and RAD51B proteins, the EVL:RAD51 and EVL:RAD51B ratios detected in the gel were 2.4:1 and 1.4:1, respectively (Fig. 3, *C* and *D*, *lane 7*). Therefore, we conclude that the EVL protein directly interacts with the RAD51 and RAD51B proteins.

The EVL Protein Stimulates RAD51-mediated Homologous Pairing—As shown in Fig. 4, *A* and *B*, the EVL protein bound to both ssDNA and dsDNA. A competitive DNA-binding assay revealed that the EVL protein preferentially bound to ssDNA rather than dsDNA (Fig. 4*C*). To study the EVL activity in the recombination reaction, we tested whether the EVL protein affects the RAD51-mediated homologous pairing. To do so, we performed the D-loop formation assay (Fig. 5*A*). The superhelical dsDNA used in this assay was prepared by a method without alkali treatment to avoid denaturation of the double helix of the dsDNA (15). As shown in Fig. 5, *B* (*lanes 2–4*) and *C*, the EVL

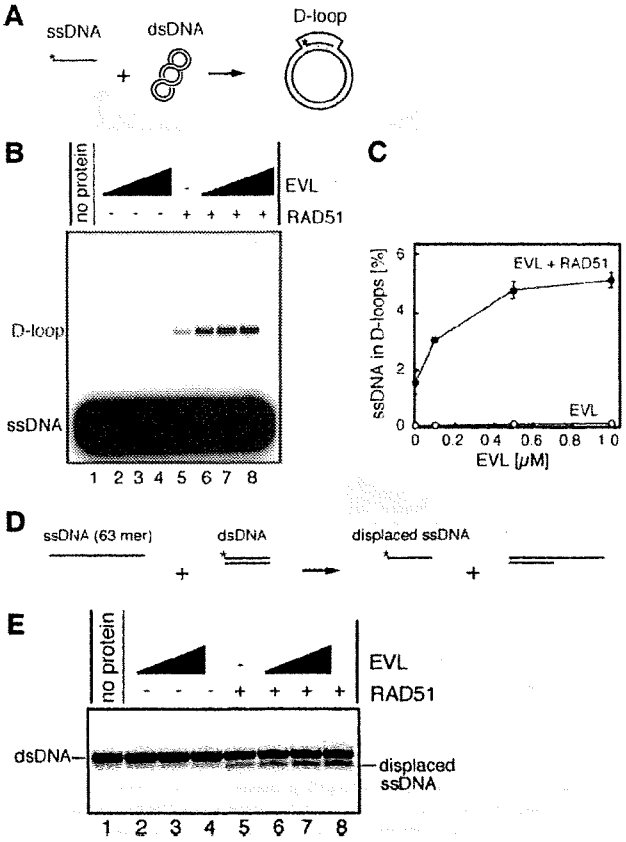

FIGURE 5. **The EVL protein stimulates the RAD51-mediated homologous pairing.** *A*, a schematic representation of the D-loop formation assay. *Asterisks* indicate the ^{32}P-labeled end of the 50-mer ssDNA. *B*, the D-loop formation assay. The reactions were conducted without the RAD51 protein (*lanes 1–4*) or with the RAD51 protein (0.1 μM) (*lanes 5–8*) in the presence of increasing amounts of the EVL protein. The EVL concentrations were 0 μM (*lanes 1* and *5*), 0.1 μM (*lanes 2* and *6*), 0.5 μM (*lanes 3* and *7*), and 1 μM (*lanes 4* and *8*). *C*, graphic representation of the experiments shown in *B*. *Closed* and *open circles*, experiments with and without the RAD51 protein, respectively. *D*, a schematic representation of the homologous pairing assay with oligonucleotides. The *asterisks* indicate the ^{32}P-labeled end of the 32-mer DNA strand. *E*, the homologous pairing assay. The reactions were conducted without the RAD51 protein (*lanes 1–4*) or with the RAD51 protein (1 μM) (*lanes 5–8*) in the presence of increasing amounts of the EVL protein. The EVL concentrations were 0 μM (*lanes 1* and *5*), 0.5 μM (*lanes 2* and *6*), 1 μM (*lanes 3* and *7*), and 2 μM (*lanes 4* and *8*).

protein alone did not promote D-loop formation. However, intriguingly, the amount of D-loops formed by the RAD51 protein synergistically increased, in an EVL concentration-dependent manner (Fig. 5, *B* (*lanes 5–8*) and *C*). Therefore, the EVL protein may have an activator function in homologous pairing by the RAD51 protein.

To confirm this EVL-mediated activation of homologous pairing, we performed the homologous pairing assay with short oligonucleotides (Fig. 5*D*). In this assay, a 63-mer ssDNA and a homologous 32-mer dsDNA were used as substrates. In the reaction, the ^{32}P-labeled 32-mer strand, which contains a sequence identical to that of the 63-mer ssDNA, is displaced from the dsDNA, as a consequence of the homologous pairing and subsequent strand exchange reactions by RAD51. As shown in Fig. 5*E* (*lanes 5–8*), the EVL protein enhanced the RAD51-mediated homologous pairing between the 63-mer ssDNA and the homologous 32-mer dsDNA. The displaced ^{32}P-labeled 32-mer product was not detected when the RAD51 protein was omitted from the reaction mixture (Fig. 5*E*, *lanes 2–4*), suggesting that the EVL protein alone did not promote homologous pairing. These results obtained from two independent homologous pairing assays are perfectly consistent; therefore, we conclude that the EVL protein stimulates the RAD51-mediated homologous pairing *in vitro*.

The EVL Protein Stimulates RAD51-mediated Strand Exchange—After homologous pairing, the RAD51 protein promotes a long tract of strand exchange, probably for the fine matching of homologous sequences. We next tested whether the EVL protein affects the RAD51-mediated strand exchange with long DNA substrates. In this assay, φX174 phage circular ssDNA (5,386 bases) and linearized φX174 dsDNA (5,386 base pairs) were used as DNA substrates (Fig. 6*A*). RPA is required for the efficient promotion of the strand exchange reaction by the RAD51 protein, but this RPA-dependent stimulation of strand exchange was not significant when the ssDNA was pre-incubated with RPA before the RAD51-ssDNA binding. This suppressive effect of RPA is considered to be overcome by the RAD51-binding proteins (11).

We then conducted the strand exchange reaction under the suppressive conditions with RPA. Interestingly, the EVL protein clearly enhanced the RAD51-mediated strand exchange, in a concentration-dependent manner (Fig. 6, *B* and *C*). No products were observed when the reactions were conducted without the RAD51 protein (Fig. 6*B*, *lane 7*), suggesting that the EVL protein itself did not possess the strand exchange activity. A time course experiment also revealed significant enhancement of the RAD51-mediated strand exchange by the EVL protein (Fig. 6*D*). Therefore, the EVL protein may be a novel stimulation factor for RAD51-mediated strand exchange as well as homologous pairing.

We next tested the effects of the reaction orders on strand exchange. As shown in Fig. 6*E* (*lanes 2* and *3*), the EVL-mediated stimulation of strand exchange was clearly observed when all three proteins, RAD51, RPA, and EVL, were mixed before the addition of ssDNA. Similarly, substantial enhancement was observed when the RAD51 protein was incubated with ssDNA followed by the addition of the RPA and EVL proteins (Fig. 6*E*, *lanes 4* and *5*). A small but clear increase in the products was detected when the RAD51 protein, RPA, and ssDNA were mixed before the addition of the EVL protein (Fig. 6*E*, *lanes 6* and *7*). Preincubation of the RAD51 and EVL proteins with ssDNA before the addition of RPA also enhanced the strand exchange (Fig. 6*E*, *lanes 8* and *9*). Therefore, the EVL protein actually stimulates the RAD51-mediated strand exchange in various reaction orders, although the stimulation efficiencies significantly depend on the reaction order.

It should be noted that the partial ssDNA annealing products (indicated by *asterisks* in Fig. 6) generated by the RAD51 protein were detected under the reaction conditions used in the present study (30 °C). This RAD51-dependent ssDNA annealing product was resolved by heating and was not significantly formed when the reactions were performed at 37 °C (supplemental Fig. 2).

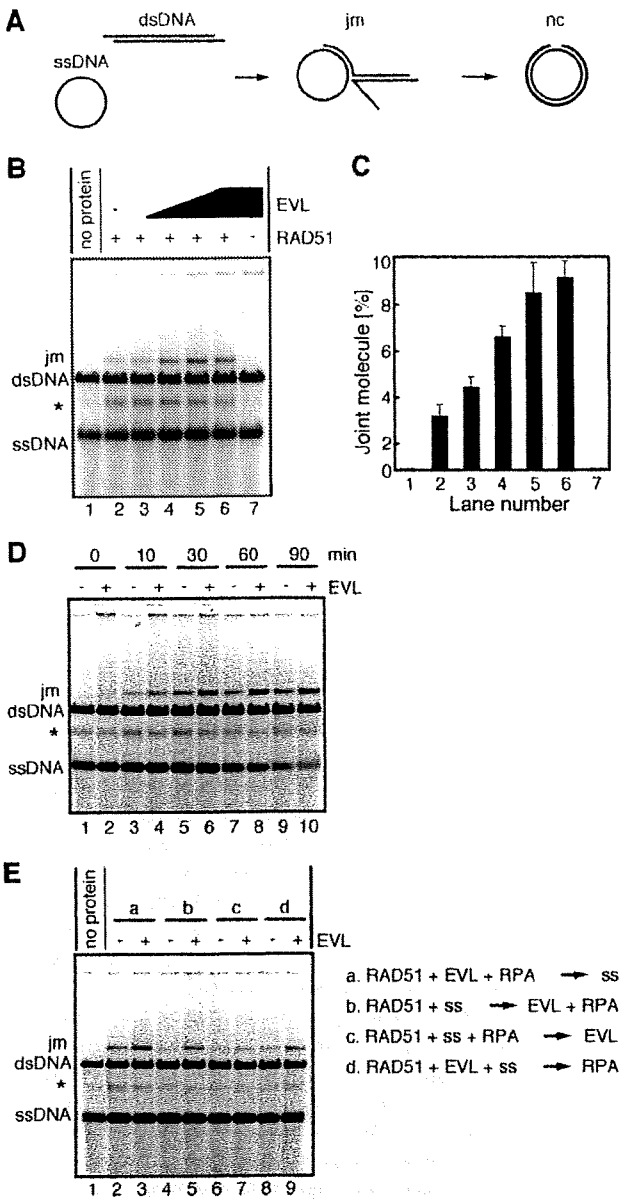

FIGURE 6. **The EVL protein stimulates the RAD51-mediated strand exchange.** *A*, a schematic representation of the strand exchange reaction. The two reaction products, joint molecule and nicked circular DNAs, are denoted as *jm* and *nc*, respectively. *B*, the RAD51 protein (1 μM) and RPA (1 μM) were incubated with the indicated amounts of the EVL protein at 30 °C for 10 min. After this incubation, ϕX174 circular ssDNA (20 μM) was added to the reaction mixture, which was incubated at 30 °C for 10 min. The reactions were then initiated by the addition of ϕX174 linear dsDNA (20 μM) and were continued at 30 °C for 60 min. The deproteinized products were separated by 1% agarose gel electrophoresis and were visualized by SYBR Gold (Invitrogen) staining. The *asterisk* indicates the self-annealing products of the ssDNA. The EVL concentrations were 0 μM (*lanes 1 and 2*), 0.25 μM (*lane 3*), 0.5 μM (*lane 4*), 1 μM (*lane 5*), and 2 μM (*lanes 6 and 7*). *Lane 7*, a control experiment without the RAD51 protein. *C*, graphic representation of the experiments shown in *B*. The band intensities of the joint molecule DNA products were quantified, and the average values of three independent experiments are shown with the S.D. values. *D*, time course experiment. The RAD51 protein (1 μM) and RPA (1 μM) were incubated with the EVL protein (1 μM) at 30 °C for 10 min. After this incubation, ϕX174 circular ssDNA (20 μM) was added to the reaction mixture, which was further incubated at 30 °C for 10 min. The reactions were then initiated by the addition of ϕX174 linear dsDNA (20 μM) and were continued for the indicated times. The deproteinized products were separated by 1% agarose gel electrophoresis and were visualized by SYBR Gold staining. *E*, the strand exchange assay with various reaction orders. The RAD51 protein (1 μM), RPA (1 μM), the EVL protein (1 μM), and ssDNA were incubated in the indicated reaction orders at 30 °C for 10 min. The reactions were then initiated by the addition of ϕX174 linear dsDNA (20 μM) and were continued at 30 °C for 60 min. The deproteinized products were separated by 1% agarose gel electrophoresis and were visualized by SYBR Gold staining. The *asterisk* indicates the self-annealing products of the ssDNA.

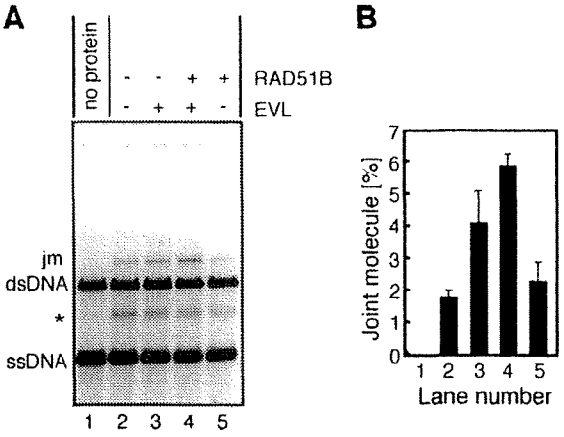

FIGURE 7. **The EVL protein further stimulates the RAD51-mediated strand exchange in the presence of the RAD51B protein.** *A*, the RAD51 protein (1 μM) and RPA (1 μM) were incubated with the EVL protein (0.5 μM) and/or the RAD51B protein (0.5 μM) at 30 °C for 10 min. After this incubation, ϕX174 circular ssDNA (20 μM) was added to the reaction mixture, which was further incubated at 30 °C for 10 min. The reactions were then initiated by the addition of ϕX174 linear dsDNA (20 μM) and were continued for 60 min. The deproteinized products were separated by 1% agarose gel electrophoresis and were visualized by SYBR Gold staining. The *asterisk* indicates the self-annealing products of the ssDNA. The EVL concentrations were 0 μM (*lanes 1, 2, and 5*) and 0.5 μM (*lanes 3 and 4*). The RAD51B protein concentrations were 0 μM (*lanes 1–3*) and 0.5 μM (*lanes 4 and 5*). *B*, graphic representation of the experiments shown in *A*. The band intensities of the joint molecule DNA products (*jm*) were quantified, and the average values of three independent experiments are shown with the S.D. values.

The RAD51B Protein Enhances RAD51-mediated Strand Exchange with the EVL Protein—We next tested whether the RAD51B protein affects RAD51-mediated strand exchange in the presence of the EVL protein, because the RAD51B protein interacts with the EVL protein (Fig. 3, *B* and *D*). The RAD51B protein was added to the reaction mixture in the presence or absence of the EVL protein. We found that the RAD51B protein stimulated RAD51-mediated strand exchange in the presence of the EVL protein (Fig. 7, *A* (*lane 4*) and *B*). In contrast, the RAD51B-dependent stimulation was not observed in the absence of the EVL protein (Fig. 7, *A* (*lane 5*) and *B*). Therefore, the RAD51B protein enhances the RAD51-mediated recombination reaction only in the presence of the EVL protein.

The EVL Protein Promotes Annealing between ssDNA Molecules—We found that the EVL protein possesses robust ssDNA annealing activity. In this assay, complementary ssDNA 49-mers were used as the substrates. As shown in Fig. 8, *A–D*, the EVL protein alone promoted annealing between complementary strands. In contrast, the RAD51B protein alone did not exhibit annealing activity (Fig. 8, *E* (*lanes 2–4*) and *F*). Interestingly, the EVL-mediated annealing was significantly enhanced by the RAD51B protein (Fig. 8, *E* (*lanes 5–8*) and *F*). These results indicated that the EVL protein may be a novel factor that

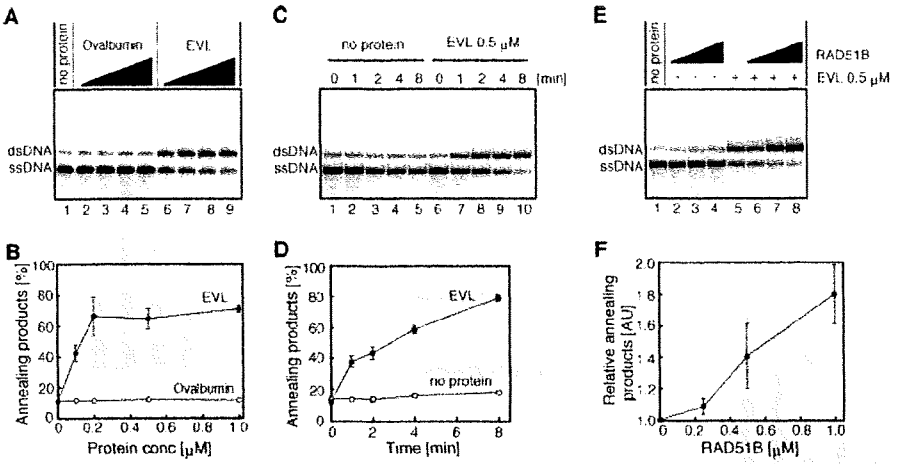

FIGURE 8. **ssDNA annealing activity of the EVL protein.** *A*, protein titration. The EVL protein was first complexed with 2 μM ssDNA, followed by the addition of a complementary ssDNA. The reactions were conducted at 30 °C for 8 min. *Lane 1*, a control experiment without protein; *lanes 6–9*, experiments with the EVL protein. The EVL concentrations were 0 μM (*lane 1*), 0.1 μM (*lane 6*), 0.2 μM (*lane 7*), 0.5 μM (*lane 8*), and 1 μM (*lane 9*). *Lanes 2–5*, negative control experiments with ovalbumin; the amounts of protein were the same as those of the EVL protein, in terms of weight. *B*, graphical representation of the experiments shown in *A*. The band intensities of the annealing products were quantified, and the average values of three independent experiments are shown with the S.D. values. *Closed circles* and *open circles*, experiments with the EVL protein and with ovalbumin, respectively. *C*, time course. *Lanes 1–5*, negative control experiments without the EVL protein. *Lanes 6–10*, experiments with the EVL protein (0.5 μM). Reaction times were 0 min (*lanes 1* and *6*), 1 min (*lanes 2* and *7*), 2 min (*lanes 3* and *8*), 4 min (*lanes 4* and *9*), and 8 min (*lanes 5* and *10*). *D*, graphical representation of the experiments shown in *C*. The band intensities of the annealing products were quantified, and the average values of three independent experiments are shown with the S.D. values. *Closed circles* and *open circles*, experiments with and without the EVL protein, respectively. *E*, effect of the RAD51B protein. The EVL protein was preincubated with or without the RAD51B protein, followed by an incubation with 2 μM ssDNA. The reactions were initiated by the addition of a complementary ssDNA and were conducted at 30 °C for 8 min. *Lanes 1–4*, experiments without the EVL protein; *lanes 5–8*, experiments with the EVL protein. The RAD51B concentrations were 0 μM (*lanes 1* and *5*), 0.25 μM (*lanes 2* and *6*), 0.5 μM (*lanes 3* and *7*), and 1 μM (*lanes 4* and *8*). *F*, graphical representation of the experiments shown in *E*. The band intensities of the annealing products, relative to the experiment in the absence of the RAD51B protein, were quantified, and the average values of three independent experiments are shown with the S.D. values.

functions in the HRR pathway and that the RAD51B protein stimulates the EVL-mediated recombination reactions.

DISCUSSION

The human EVL protein is a member of the Ena/Vasp family, which reportedly functions in cytoplasmic actin dynamics (48). In the present study, we discovered an unexpected function of the EVL protein in the HRR pathway. Specifically, we found that the EVL protein (i) directly binds to the RAD51 and RAD51B proteins, (ii) functions in DSB repair, probably in the RAD51 assembly step on DSB sites, (iii) stimulates RAD51-mediated homologous pairing and strand exchange, and (iv) preferentially binds to ssDNA and promotes ssDNA annealing. We also found that (v) the RAD51B protein enhances the EVL-dependent strand exchange stimulation and ssDNA annealing reactions. These EVL activities discovered in the present study strongly suggest that the EVL protein is a novel activator for the RAD51-mediated homologous recombination reaction.

The biochemical properties of the EVL protein presented here are surprisingly similar to those of the RAD52 protein, which is a prominent RAD51 activator in eukaryotes. The RAD52 protein directly binds to the RAD51 protein (13–15) and stimulates RAD51-mediated homologous pairing (18) and strand exchange (53–55). The RAD52 protein itself possesses robust ssDNA annealing activity (56–59). These functional similarities between the EVL and RAD52 proteins imply that they may have overlapping functions in cells.

In the present study, we found that MMC sensitivity in the EVL knockdown cells was not as remarkable as the MMC sensitivity of the RAD51B knockdown cells. This fact implies that a factor(s) that complements the EVL function may exist. The RAD52 protein, which shares significant biochemical similarity with the EVL protein, may be a factor. In addition, two more paralogs of the EVL protein, MENA and VASP, exist in humans (48) and may also contribute to the functional redundancy of the EVL protein.

The RAD52 knock-out chicken DT40 cells reportedly did not exhibit defects in DSB repair (60). The cells with the double knock-out of the RAD52 and XRCC2 proteins were significantly defective in the HRR pathway (61), indicating that the RAD52 protein has an overlapping function with the XRCC2 protein. The XRCC2 protein forms the BCDX2 complex, which is composed of the RAD51B, RAD51C, RAD51D, and XRCC2 proteins (62, 63), and like the EVL and RAD52 proteins, the BCDX2 complex possesses robust ssDNA annealing activity (64). Therefore, redundant annealing activities may be required in the HRR pathway in higher eukaryotes. The RAD52-mediated annealing is suggested to be important in the second end capture step, just after homologous pairing and strand exchange (65). Therefore, the EVL protein may also function in the second end capture step, in addition to the RAD51 assembly and homologous pairing/strand exchange steps. It is intriguing to study the functional interactions between these ssDNA annealing proteins, such as RAD52, BCDX2, and EVL-RAD51B.

We found that the EVL protein was highly expressed in MCF7 cells. However, we noticed that EVL expression was very low in other cells, such as RPE, HT1080, T47D, HepG2, and HCT116 (data not shown). The rat EVL homologue is reportedly expressed in brain, lung, spleen, thymus, and testis but not in liver, muscle, and prostate (66). Given that the EVL protein is a novel recombination activator for the RAD51-dependent HRR pathway, it may not constitutively function like the RAD51 and RAD51B proteins. The EVL protein may be required for repairing specific DNA lesions in certain tissues or cells, and it may cause tumor malignancy due to inappropriate recombination activation by its overexpression in certain types of tumor cells. The MCF7 cell line,

which robustly expresses the EVL protein, was derived from a breast cancer tumor. Intriguingly, the abnormal expression of the EVL mRNA was also found in another breast cancer tumor (49). Given that EVL overexpression is a source for the malignancy of tumor cells, such as breast cancer, the EVL protein may be a potential target of anti-cancer treatments.

Acknowledgments—We thank Dr. W. Kagawa (RIKEN) for critical reading of the manuscript and also thank the Cs-137 γ-ray Irradiation Facilities for Biological Research, Department of Nuclear Engineering and Management, Graduate School of Engineering, University of Tokyo.

REFERENCES

1. Weinstock, D. M., Richardson, C. A., Elliott, B., and Jasin, M. (2006) *DNA Repair* **5,** 1065–1074
2. Agarwal, S., Tafel, A. A., and Kanaar, R. (2006) *DNA Repair* **5,** 1075–1081
3. Wyman, C., and Kanaar, R. (2006) *Annu. Rev. Genet.* **40,** 363–383
4. Sung, P., and Klein, H. (2006) *Nat. Rev. Mol. Cell Biol.* **7,** 739–750
5. West, S. C. (2003) *Nat. Rev. Mol. Cell Biol.* **4,** 435–445
6. Sung, P. (1994) *Science* **265,** 1241–1243
7. Baumann, P., Benson, F. E., and West, S. C. (1996) *Cell* **87,** 757–766
8. Maeshima, K., Morimatsu, K., and Horii, T. (1996) *Genes Cells* **1,** 1057–1068
9. Gupta, R. C., Bazemore, L. R., Golub, E. I., and Radding, C. M. (1997) *Proc. Natl. Acad. Sci. U. S. A.* **94,** 463–468
10. Symington, L. S. (2002) *Microbiol. Mol. Biol. Rev.* **66,** 630–670
11. Sung, P., Krejci, L., Van Komen, S., and Sehorn, M. G. (2003) *J. Biol. Chem.* **278,** 42729–42732
12. San Filippo, J., Sung, P., and Klein, H. (2008) *Annu. Rev. Biochem.* **77,** 229–257
13. Shen, Z., Cloud, K. G., Chen, D. J., and Park, M. S. (1996) *J. Biol. Chem.* **271,** 148–152
14. Kurumizaka, H., Aihara, H., Kagawa, W., Shibata, T., and Yokoyama, S. (1999) *J. Mol. Biol.* **291,** 537–548
15. Kagawa, W., Kurumizaka, H., Ikawa, S., Yokoyama, S., and Shibata, T. (2001) *J. Biol. Chem.* **276,** 35201–35208
16. Golub, E. I., Kovalenko, O. V., Gupta, R. C., Ward, D. C., and Radding, C. M. (1997) *Nucleic Acids Res.* **25,** 4106–4110
17. Tanaka, K., Hiramoto, T., Fukuda, T., and Miyagawa, K. (2000) *J. Biol. Chem.* **275,** 26316–26321
18. Benson, F. E., Baumann, P., and West, S. C. (1998) *Nature* **391,** 401–404
19. Sigurdsson, S., Van Komen, S., Petukhova, G., and Sung, P. (2002) *J. Biol. Chem.* **277,** 42790–42794
20. Mazina, O. M., and Mazin, A. V. (2004) *J. Biol. Chem.* **279,** 52042–52051
21. Wesoly, J., Agarwal, S., Sigurdsson, S., Bussen, W., Van Komen, S., Qin, J., van Steeg, H., van Benthem, J., Wassenaar, E., Baarends, W. M., Ghazvini, M., Tafel, A. A., Heath, H., Galjart, N., Essers, J., Grootegoed, J. A., Arnheim, N., Bezzubova, O., Buerstedde, J. M., Sung, P., and Kanaar, R. (2006) *Mol. Cell. Biol.* **26,** 976–989
22. Kovalenko, O. V., Golub, E. I., Bray-Ward, P., Ward, D. C., and Radding, C. M. (1997) *Nucleic Acids Res.* **25,** 4946–4953
23. Modesti, M., Budzowska, M., Baldeyron, C., Demmers, J. A., Ghirlando, R., and Kanaar, R. (2007) *Mol. Cell* **28,** 468–481
24. Wiese, C., Dray, E., Groesser, T., San Filippo, J., Shi, I., Collins, D. W., Tsai, M. S., Williams, G. J., Rydberg, B., Sung, P., and Schild, D. (2007) *Mol. Cell* **28,** 482–490
25. Davies, A. A., Masson, J. Y., McIlwraith, M. J., Stasiak, A. Z., Stasiak, A., Venkitaraman, A. R., and West, S. C. (2001) *Mol. Cell* **7,** 273–282
26. Pellegrini, L., Yu, D. S., Lo, T., Anand, S., Lee, M., Blundell, T. L., and Venkitaraman, A. R. (2002) *Nature* **420,** 287–293
27. Yang, H., Jeffrey, P. D., Miller, J., Kinnucan, E., Sun, Y., Thoma, N. H., Zheng, N., Chen, P. L., Lee, W. H., and Pavletich, N. P. (2002) *Science* **297,** 1837–1848
28. Esashi, F., Christ, N., Gannon, J., Liu, Y., Hunt, T., Jasin, M., and West, S. C. (2005) *Nature* **434,** 598–604
29. Galkin, V. E., Esashi, F., Yu, X., Yang, S., West, S. C., and Egelman, E. H. (2005) *Proc. Natl. Acad. Sci. U. S. A.* **102,** 8537–8542
30. Shivji, M. K., Davies, O. R., Savill, J. M., Bates, D. L., Pellegrini, L., and Venkitaraman, A. R. (2996) *Nucleic Acids Res.* **34,** 4000–4011
31. Davies, O. R., and Pellegrini, L. (2007) *Nat. Struct. Mol. Biol.* **14,** 475–483
32. Esashi, F., Galkin, V. E., Yu, X., Egelman, E. H., and West, S. C. (2007) *Nat. Struct. Mol. Biol.* **14,** 468–474
33. Petalcorin, M. I., Galkin, V. E., Yu, X., Egelman, E. H., and Boulton, S. J. (2007) *Proc. Natl. Acad. Sci. U. S. A.* **104,** 8299–8304
34. Mazloum, N., Zhou, Q., and Holloman, W. K. (2007) *Biochemistry* **46,** 7163–7173
35. Mazloum, N., Zhou, Q., and Holloman, W. K. (2007) *Proc. Natl. Acad. Sci. U. S. A.* **105,** 524–529
36. Albala, J. S., Thelen, M. P., Prange, C., Fan, W., Christensen, M., Thompson, L. H., and Lennon, G. G. (1997) *Genomics* **46,** 476–479
37. Rice, M. C., Smith, S. T., Bullrich, F., Havre, P., and Kmiec, E. B. (1997) *Proc. Natl. Acad. Sci. U. S. A.* **94,** 7417–7422
38. Cartwright, R., Dunn, A. M., Simpson, P. J., Tambini, C. E., and Thacker, J. (1998) *Nucleic Acids Res.* **26,** 1653–1659
39. Takata, M., Sasaki, M. S., Sonoda, E., Fukushima, T., Morrison, C., Albala, J. S., Swagemakers, S. M. A., Kanaar, R., Thompson, L. H., and Takeda, S. (2000) *Mol. Cell. Biol.* **20,** 6476–6482
40. Bleuyard, J. Y., Gallego, M. E., Savigny, F., and White, C. I. (2005) *Plant J.* **41,** 533–545
41. Hatanaka, A., Yamazoe, M., Sale, J. E., Takata, M., Yamamoto, K., Kitao, H., Sonoda, E., Kikuchi, K., Yonetani, Y., and Takeda, S. (2005) *Mol. Cell. Biol.* **25,** 1124–1134
42. Osakabe, K., Abe, K., Yamanouchi, H., Takyuu, T., Yoshioka, T., Ito, Y., Kato, T., Tabata, S., Kurei, S., Yoshioka, Y., Machida, Y., Seki, M., Kobayashi, M., Shinozaki, K., Ichikawa, H., and Toki, S. (2005) *Plant Mol. Biol.* **57,** 819–833
43. Yonetani, Y., Hochegger, H., Sonoda, E., Shinya, S., Yoshikawa, H., Takeda, S., and Yamazoe, M. (2005) *Nucleic Acids Res.* **33,** 4544–4552
44. Date, O., Katsura, M., Ishida, M., Yoshihara, T., Kinomura, A., Sueda, T., and Miyagawa, K. (2006) *Cancer Res.* **66,** 6018–6024
45. Sigurdsson, S., Van, Komen, S., Bussen, W., Schild, D., Albala, J. S., and Sung, P. (2001) *Genes Dev.* **15,** 3308–3318
46. Lio, Y. C., Mazin, A. V., Kowalczykowski, S. C., and Chen, D. J. (2003) *J. Biol. Chem.* **278,** 2469–2478
47. Yokoyama, H., Kurumizaka, H., Ikawa, S., Yokoyama, S., and Shibata, S. (2003) *J. Biol. Chem.* **278,** 2767–2772
48. Kwiatkowski, A. V., Gertler, F. B., and Loureiro, J. J. (2003) *Trends Cell Biol.* **13,** 386–392
49. Hu, L. D., Zou, H. F., Zhan, S. X., and Cao, K. M. (2008) *Oncol. Rep.* **19,** 1015–1020
50. Ishida, T., Takizawa, Y., Sakane, I., and Kurumizaka, H. (2008) *Genes Cells* **13,** 91–103
51. Kinebuchi, T., Kagawa, W., Enomoto, R., Tanaka, K., Miyagawa, K., Shibata, T., Kurumizaka, H., and Yokoyama, S. (2004) *Mol. Cell* **14,** 363–374
52. Henricksen, L. A., Umbricht, C. B., and Wold, M. S. (1994) *J. Biol. Chem.* **269,** 11121–11132
53. Sung, P. (1997) *J. Biol. Chem.* **272,** 28194–28197
54. New, J. H., Sugiyama, T., Zaitseva, E., and Kowalczykowski, S. C. (1998) *Nature* **391,** 407–410
55. Shinohara, A., and Ogawa, T. (1998) *Nature* **391,** 404–407
56. Mortensen, U. H., Bendixen, C., Sunjevaric, I., and Rothstein, R. (1996) *Proc. Natl. Acad. Sci. U. S. A.* **93,** 10729–10734
57. Reddy, G., Golub, E. I., and Radding, C. M. (1997) *Mutat. Res.* **377,** 53–59
58. Sugiyama, T., New, J. H., and Kowalczykowski, S. C. (1998) *Proc. Natl. Acad. Sci. U. S. A.* **95,** 6049–6054
59. Kagawa, W., Kagawa, A., Saito, K., Ikawa, S., Shibata, T., Kurumizaka, H., and Yokoyama, S. (2008) *J. Biol. Chem.* **283,** 24264–24273
60. Yamaguchi-Iwai, Y., Sonoda, E., Buerstedde, J. M., Bezzubova, O., Morrison, C., Takata, M., Shinohara, A., and Takeda, S. (1998) *Mol. Cell. Biol.* **18,** 6430–6435
61. Fujimori, A., Tachiiri, S., Sonoda, E., Thompson, L. H., Dhar, P. K.,

Hiraoka, M., Takeda, S., Zhang, Y., Reth, M., and Takata, M. (2001) *EMBO J.* **20,** 5513–5520
62. Masson, J. Y., Tarsounas, M. C., Stasiak, A. Z., Stasiak, A., Shah, R., McIlwraith, M. J., Benson, F. E., and West, S. C. (2001) *Genes Dev.* **15,** 3296–3307
63. Schild, D., Lio, Y. C., Collins, D. W., Tsomondo, T., and Chen, D. (2000) *J. Biol. Chem.* **275,** 16443–16449
64. Yokoyama, H., Sarai, N., Kagawa, W., Enomoto, R., Shibata, T., Kurumizaka, H., and Yokoyama, S. (2004) *Nucleic Acids Res.* **32,** 2556–2565
65. McIlwraith, M. J., and West, S. C. (2008) *Mol. Cell* **29,** 510–516
66. Ohta, S., Mineta, T., Kimoto, M., and Tabuchi, K. (1997) *Biochem. Biophys. Res. Commun.* **237,** 307–312

ARTICLE IN PRESS

Cancer Letters xxx (2010) xxx–xxx

Contents lists available at ScienceDirect

Cancer Letters

journal homepage: www.elsevier.com/locate/canlet

Edaravone, a known free radical scavenger, enhances X-ray-induced apoptosis at low concentrations

N. Sasano [a,b], A. Enomoto [b], Y. Hosoi [c], Y. Katsumura [d], Y. Matsumoto [e], A. Morita [f], K. Shiraishi [a], K. Miyagawa [b], H. Igaki [a], K. Nakagawa [a,*]

[a] Department of Radiology, Graduate School of Medicine, The University of Tokyo, 7-3-1, Hongo, Bunkyo-ku, Tokyo 113-8655, Japan
[b] Laboratory of Molecular Radiology, Center for Disease Biology and Integrative Medicine, Faculty of Medicine, The University of Tokyo, 7-3-1, Hongo, Bunkyo-ku, Tokyo 113-0033, Japan
[c] School of Health Sciences, Faculty of Medicine, Niigata University, 1, Asahimachi-dori, Niigata, Niigata 951-8510, Japan
[d] Nuclear Engineering Research Laboratory, Graduate School of Engineering, The University of Tokyo, The University of Tokyo, 7-3-1, Hongo, Bunkyo-ku, Tokyo 113-0033, Japan
[e] Mass Transmutation Engineering Division, Research Laboratory for Nuclear Reactors, Tokyo Institute of Technology, 2-12-1, Oh-Okayama, Meguro-ku, Tokyo 152-0033, Japan
[f] Department of Applied Biological Science, Faculty of Science and Technology, Tokyo University of Science, 1-3, Kagurazaka, Shinjuku-ku, Tokyo 162-8601, Japan

ARTICLE INFO

Article history:
Received 13 October 2009
Received in revised form 19 December 2009
Accepted 23 December 2009
Available online xxxx

Keywords:
Edaravone
Radiosensitizer
Apoptosis
p53

ABSTRACT

Edaravone has been reported to have a radioprotective effect at high concentrations. We now report that a lower dose of edaravone enhanced X-ray-induced apoptosis of some cell lines harboring p53 wild-type status, such as MOLT-4, Nalm-6, and HepG2. The knock-down of p53 using siRNA in MOLT-4 cells abolished the radiosensitizing effect of edaravone. Enhanced phosphorylations of p53 at Ser 15 and Ser 20 and up-regulation of PUMA, a p53 target protein, were observed after X-irradiation in the presence of edaravone. We conclude that the low dose of edaravone sensitized cells to X-irradiation by promoting the p53-dependent apoptotic signaling pathway.

1. Introduction

Edaravone (MCI-186; 3-methyl-1-phenyl-2-pyrazolin-5-one) is a drug widely used clinically for the treatment of acute cerebral infarction [1] and is known to scavenge free radicals as an electron donor [2]. We previously reported that in the human T-cell leukemia cell line, MOLT-4, 3 mg/ml of edaravone suppressed X-ray-induced apoptosis by inhibiting both reactive oxygen species (ROS) and p53 [3]. The MOLT-4 cell line is highly sensitive to X-rays and undergoes p53- and caspase-dependent apoptosis, showing nuclear condensation and DNA fragmentation [4]. p53 is a well-studied transcription factor associated with the determination of the cells to undergo apoptosis or other fates after DNA damage. After DNA damage, p53 stability is increased by phosphorylation, and the accumulated p53 induces the transcription of its target genes [5], including the p53-upregulated modulator of apoptosis (PUMA). PUMA is a BH3-only protein belonging to the Bcl-2 family that regulates apoptosis and plays a key functional role in the process of p53-mediated apoptosis [6–9]. Overexpressing a dominant-negative form of p53 in MOLT-4 cells results in resistance to radiation-induced apoptosis [10].

Various compounds have been reported to be effective as radiosensitizers, such as wortmannin. Wortmannin is an extensively studied inhibitor of the phosphatidylinositol 3-kinase family, ataxia telangiectasia mutated (ATM) and DNA-dependent protein kinase (DNA-PK). Wortmannin has also been reported to enhance X-ray-induced apoptosis through the inhibition of DNA repair [11,12]. Tomita et al. [13] also demonstrated that wortmannin enhances

* Corresponding author.
E-mail address: nakagawa-rad@umin.ac.jp (K. Nakagawa).

0304-3835/$ - see front matter © 2009 Elsevier Ireland Ltd. All rights reserved.
doi:10.1016/j.canlet.2009.12.020

Please cite this article in press as: N. Sasano et al., Edaravone, a known free radical scavenger, enhances X-ray-induced apoptosis at low concentrations, Cancer Lett. (2010), doi:10.1016/j.canlet.2009.12.020

X-ray-induced apoptosis possibly through the JNK/SAPK pathway in MOLT-4 cells.

Because the clinical concentration of edaravone in human blood is estimated to be approximately 1000-fold lower than that used in the previous study [14], we sought to determine the effect of lower concentrations of edaravone on X-ray-induced apoptosis. The presumption was that lower concentrations of edaravone would show a milder radioprotective effect. However, contrary to our expectations, we found that even a lower dose of edaravone enhanced the X-ray-induced apoptosis through the p53 pathway.

2. Materials and methods

2.1. Cell culture

Human T-cell leukemia MOLT-4 cells, MOLT-4 stable transfectants overexpressing short hairpin (sh)-type p53 small interfering RNA (siRNA) (p53 knock-down MOLT-4), human pre-B-cell leukemia Nalm-6 cells, and human hepatocellular carcinoma (HepG2) cells were cultured in Dulbecco's Modified Eagle Medium (Sigma) containing 5% fetal bovine serum (Hyclone) and antibiotics (100 units/ml of penicillin/streptomycin), and incubated at 37 °C in a humidified atmosphere of 5% CO_2 and 95% air. To generate p53 knock-down MOLT-4 cells, MOLT-4 cells were transfected by electroporation (Gene Pulsar II, Bio-Rad; 0.25 kV, 950 microfarads) with the ApaLI-linearized vectors (GeneSuppressor System, p53 siRNA plasmid and the negative control shRNA plasmid, IMGENEX), and selected on 0.16% soft agar culture containing 0.8 mg/ml G418 for 3 weeks.

2.2. Chemicals

Edaravone was kindly provided by the Mitsubishi Tanabe Pharma Corporation (Tokyo, Japan). Edaravone (52.5 mg) was dissolved in 192.5 μl of 2 M NaOH and 1.05 ml of DDW, and then adjusted to pH 8.8 with 2 M HCl. Finally, physiological saline was added to adjust the final concentration of edaravone to 30 mg/ml. Edaravone was added to the cells 5 min before X-irradiation.

2.3. X-irradiation

X-irradiation was performed with an X-ray generator (Pantak HF 350, Shimadzu) at 200 kVp and 20 mA, with a filter of 0.5 mm Cu and 1 mm Al, and at a dose rate of 1.35–1.40 Gy/min.

2.4. Dye exclusion tests

One hundred microliters of cell suspension (approximately 5×10^5 cells/ml) was mixed with 25 μl of 1% erythrosin B in PBS. The numbers of stained (dead) cells and unstained (live) cells were counted and the viability (%) was calculated as follows:

Viability(%)
= (number of unstained cells/total cell number) × 100

2.5. Annexin V binding assay

The extent of apoptosis was determined by Annexin V-FITC and propidium iodine (PI) staining, using the MEBCYTO Apoptosis Kit (MBL). Flow cytometric analysis was carried out with an EPICS flow cytometer (XL System II, Beckman Coulter), using a single laser emitting excitation light at 488 nm. In the FITC/PI diparametric plot, cells in quadrant four (upper FITC/ lower PI) were considered to be in the early stage of apoptosis. More than 5000 cells were subjected to the analysis.

2.6. Quantification of intracellular ROS

The amount of intracellular ROS production was measured by chloromethyl-2′, 7′-dichlorodihydro-fluorescein diacetate (CM-H_2-DCFDA, Molecular Probes). MOLT-4 cells were incubated in the dark with approximately 5 μg/ml of probe CM-H_2-DCFDA for an hour, and the fluorescence intensity was analyzed by an EPICS flow cytometer (XL System II, Beckman Coulter) using a laser excitation and emission wavelength of 492–495 nm and 517–527 nm, respectively.

2.7. Western blotting

Cells were lysed in a SDS sample buffer (1% SDS, 3% β-mercaptoethanol, 5% glycerol, 62.5 mM Tris–HCl, pH 6.8). Proteins were separated by 10% or 15% SDS–PAGE and were transferred onto polyvinylidene difluoride membranes (Immobilon, Millipore). After blocking for 30 min in 5% skim milk in TBS (20 mM Tris–HCl, pH 7.5, 150 mM NaCl) supplemented with 0.05% Tween-20 (TBS-T), the membranes were incubated overnight at 4 °C in TBS-T containing 5% skim milk and primary antibodies. The primary antibodies were anti-p53 (clone DO-1, Santa Cruz Biotechnology), anti-phospho p53 at Ser 15 (Calbiochem), Ser 6, Ser 9, Ser 20, and Ser 392 (cell signaling), anti-cleaved caspase-3 (cell signaling), anti-caspase-7 (MBL), anti-PUMA (Calbiochem), and anti-β-actin (Sigma, AC-15). After rinsing three times with TBS-T, the membranes were incubated for 2 h at room temperature in TBS-T containing 5% skim milk and secondary antibodies conjugated with horseradish peroxidase (DAKO). The membranes were then washed three times with TBS-T, once with TBS, and developed using an ECL-plus kit (GE Healthcare). The signals were obtained by exposure to X-ray films (Hyperfilm MP, GE Healthcare).

2.8. Statistical analysis

All experiments were repeated at least three times. The results are expressed as the mean ±standard deviation (SD) of the mean. All laboratory data were evaluated according to standard statistical methods, using commercially available computer programs such as Microsoft Excel 2000. Statistical differences were determined using the Student's *t*-test. In all tests, *P* values less than 0.05 were considered statistically significant.

Please cite this article in press as: N. Sasano et al., Edaravone, a known free radical scavenger, enhances X-ray-induced apoptosis at low concentrations, Cancer Lett. (2010), doi:10.1016/j.canlet.2009.12.020

3. Results

3.1. Edaravone significantly enhances X-ray-induced cell death at low concentrations

First, the cytotoxicity of edaravone was determined by using the dye exclusion test [3]. Cell viability was examined in cultures treated with 0.15, 0.75, 1.5, 3, and 6 mg/ml edaravone. With concentrations of edaravone up to 3 mg/ml, the cell viabilities were more than 60%, which was considered acceptable (Fig. 1A). On the other hand, when treated with 6 mg/ml edaravone, cell viability was less than 30% and this was considered overly cytotoxic (Fig. 1A). These results are consistent with the previous report [3].

To determine the effect of edaravone on X-ray-induced cell death, MOLT-4 cells were treated with various concentrations of edaravone, and then subjected to 2 Gy X-irradiation 5 min later. Cell viabilities were determined 20 h after the treatment. When MOLT-4 cells were X-irradiated without edaravone, the cell viability was 36.2 ± 6.3% (Fig. 1A). When MOLT-4 cells were X-irradiated in the presence of edaravone at concentrations of 0.15, 0.75, and 1.5 mg/ml, the cell viabilities were 9.7 ± 2.1%, 5.7 ± 3.5%, and 7.2 ± 6.3%, respectively (Fig. 1A). These results were significantly lower than that in the absence of edaravone ($P < 0.05$). The enhancement of X-ray-induced cell death was observed in a time- and dose-dependent manner ($P < 0.05$) (Fig. 1B and C). These results indicate that low doses of edaravone enhanced X-ray-induced cell death. Considering the cytotoxicity of edaravone (Fig. 1A), the combined effect of these concentrations of edaravone and X-irradiation on MOLT-4 cell viability was considered supra-additive. On the other hand, when MOLT-4 cells were X-irradiated in combination with 2.7 or 3 mg/ml of edaravone, the cell viability increased significantly ($P < 0.05$) (Fig. 1A), which was compatible with the previous report [3]. Because 0.75 mg/ml of edaravone appeared to enhance X-ray-induced MOLT-4 cell death most effectively, this dose was used for all subsequent experiments in this study.

Although not as remarkable as noted in MOLT-4 cells, the radiosensitizing effect of edaravone was also observed in human pre-B-cell leukemia Nalm-6 and hepatocellular carcinoma HepG2 cells ($P < 0.05$) (Fig. 2A and B). Thus, the radiosensitizing effect of a low dose of edaravone is not limited to MOLT-4 cells, but is observed in cells with p53 wild-type status.

To determine whether DMSO (dimethylsulfoxide), another free radical scavenger, has a similar radiosensitizing effect in low doses, a dye exclusion test was performed on MOLT-4 cells treated with 0.2% or 1% DMSO, and then subjected to X-irradiation. The viability of the cells treated with 1% DMSO before X-irradiation was significantly greater than that of the cells treated only with X-irradiation ($P < 0.05$), indicating that 1% DMSO had a radioprotective effect. On the other hand, the viability of the cells treated with 0.2% DMSO before X-irradiation was almost the same as that of the cells treated only with X-irradiation (Fig. 2C). These results indicate that low doses of free radical scavengers do not always show the radiosensitizing effect.

3.2. Low dose of edaravone (0.75 mg/ml) enhances X-ray-induced MOLT-4 cell death by promoting apoptosis

To determine whether the radiosensitizing effect of edaravone is mediated by apoptosis, the effect of edaravone on the induction of apoptosis was examined by using flow cytometric studies with Annexin V-PI staining. When MOLT-4 cells were treated with either edaravone or 2 Gy X-ray, the percentages of Annexin V+/PI– cells in the early stage of apoptosis were 2.04 ± 0.21% and 12.43 ± 1.96%, respectively (Fig. 3A and C). When MOLT-4 cells were subjected to 2 Gy X-irradiation in addition to edaravone, the result was 39.57 ± 4.48% (Fig. 3B and C). This indicated that adding 0.75 mg/ml edaravone significantly increased the frequency of X-ray-induced apoptosis ($P < 0.05$), and that the combined effect of edaravone and X-irradiation was supra-additive. The next investigation was on the effect of edaravone on the activation of caspase-3 and -7, which are known as apoptotic effectors and play crucial roles in the execution of apoptosis [15]. Treatment with X-irradiation combined with edaravone resulted in an earlier induction of the active forms of caspase-3 and -7. With X-irradiation alone however, the same results were not obtained until 8 h after the treatment (Fig. 3D). These data indicate that the radiosensitizing effect of a low dose of edaravone is due to the enhancement of apoptosis.

3.3. Effects of edaravone on the production of intracellular ROS

CM-H_2-DCFDA, a fluorescence-based probe recently developed to detect the intracellular production of ROS, was used in a flow cytometry sys-

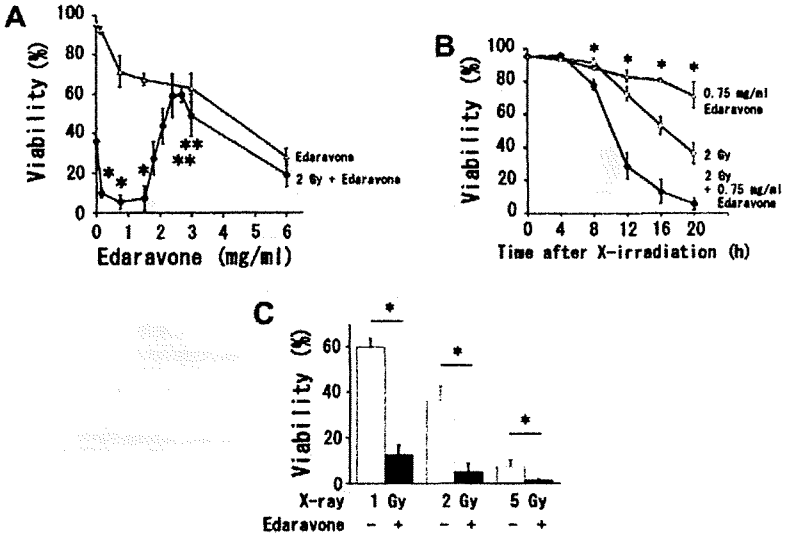

Fig. 1. Low concentrations of edaravone enhanced X-ray-induced cell death in MOLT-4 cells. (A) Cytotocixity of edaravone and effects of various concentrations of edaravone on 2 Gy X-ray-induced cell death are shown. Cell viabilities were determined 20 h after treatment with the indicated concentrations of edaravone with or without X-irradiation. *$P < 0.05$, meaning significantly lower than that of the X-irradiated cells in the absence of edaravone. **$P < 0.05$, meaning significantly higher than that of the X-irradiated cells in the absence of edaravone. (B) The time-course cell viability after treatment with 2 Gy X-irradiation and/or 0.75 mg/ml edaravone. *$P < 0.05$, meaning that the viability of the X-irradiated cells in the absence of edaravone is significantly higher than that of the X-irradiated cells in the presence of 0.75 mg/ml edaravone. (C) X-ray-dose response of cell death in the absence or presence of 0.75 mg/ml edaravone. *$P < 0.05$.

Please cite this article in press as: N. Sasano et al., Edaravone, a known free radical scavenger, enhances X-ray-induced apoptosis at low concentrations, Cancer Lett. (2010), doi:10.1016/j.canlet.2009.12.020

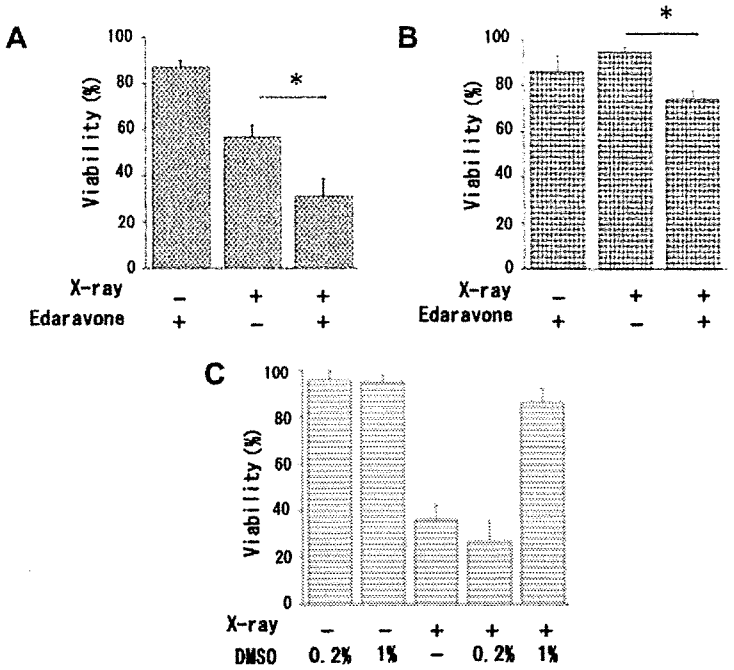

Fig. 2. Low concentrations of edaravone also enhanced X-ray-induced cell death in Nalm-6 (A) and HepG2 (B) cells. In Nalm-6 and HepG2 cells, cell viabilities were determined by dye exclusion test with erythrosine B 20 h after the treatment with 0.75 mg/ml edaravone and/or 2 Gy X-irradiation. $^{*}P < 0.05$. (C) Another free radical scavenger, DMSO, did not show the radiosensitizing effect at a low dose. Cell viability of MOLT-4 was determined 20 h after X-irradiation in the absence or presence of DMSO.

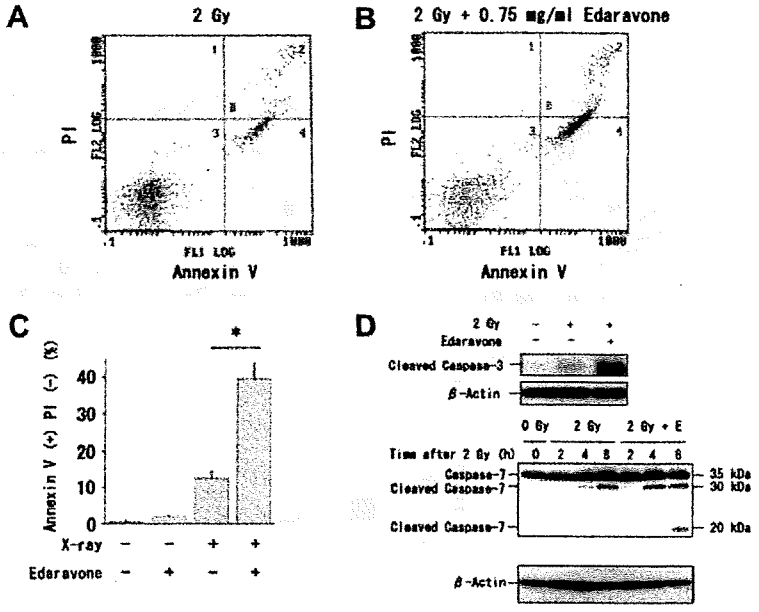

Fig. 3. A low dose of edaravone enhanced X-ray-induced apoptosis. (A–C) Apoptosis was quantified by Annexin V-PI staining. Cells were harvested 8 h after each treatment (2 Gy X-irradiation and/or 0.75 mg/ml edaravone). (A) Two Gy X-irradiation only. (B) Two Gy X-irradiation and 0.75 mg/ml edaravone. (C) The percentage of the Annexin V+/PI− cells is indicated. $^{*}P < 0.05$. (D) Cells were X-irradiated in the absence or presence of 0.75 mg/ml edaravone (E), then harvested at the indicated times. Western blot analysis was performed using anti-cleaved caspase-3 and anti-caspase-7. β-Actin as a loading control is shown.

Please cite this article in press as: N. Sasano et al., Edaravone, a known free radical scavenger, enhances X-ray-induced apoptosis at low concentrations, Cancer Lett. (2010), doi:10.1016/j.canlet.2009.12.020

tem to study the effect of edaravone on the X-ray-induced production of intracellular ROS [16]. CM-H_2-DCFDA is passively diffused into and trapped within the cells, and is deacetylated by intracellular esterases. It is subsequently oxidized to a fluorescent product in the presence of intracellular ROS. The oxidation of CM-H_2-DCFDA can be monitored as a convenient determinant of the level of intracellular oxidative stress. X-irradiation at 20 Gy induced an approximately 11-fold increase in basal CM-H_2-DCFDA fluorescence, which was significantly suppressed by adding 0.75 mg/ml edaravone 5 min before X-irradiation ($P < 0.05$) (Fig. 4A). Moreover, the suppressive effect was even greater when 3 mg/ml edaravone was added ($P < 0.05$). This result indicates that the radiosensitizing effect of edaravone is not mediated by promoting ROS generation.

3.4. p53 is involved in the radiosensitizing effect of a low dose (0.75 mg/ml) of edaravone

To determine whether p53 is involved in the radiosensitizing effect of edaravone, we used one of two stable p53 knock-down transformants, which were generated using a vector that overexpressed p53 siRNA [17]. A clone was used which showed a better suppression of p53. It was reconfirmed that this clone showed significantly lower levels of p53 expression than the wild-type MOLT-4 cells even after X-irradiation with or without edaravone (Fig. 4B). This clone was X-irradiated at 2 Gy with or without edaravone and the cells were subjected to the dye exclusion test. Differences of cell viabilities at 20 h after X-irradiation for the cells untreated or treated with edaravone were not significant, i.e., 88:63 ± 2.02% and 86.13 ± 4.75%, respectively (Fig. 4C). The suppression of p53 by siRNA abolished the radiosensitizing effect of edaravone. Therefore, these results suggest that the p53 pathway is involved in the radiosensitizing effect of edaravone. Next, the effects of edaravone were analyzed on the accumulation or phosphorylation of p53 by Western blot analysis with total or phospho-specific antibodies. The results showed that edaravone enhanced the phosphorylation of p53 at Ser 15 and Ser 20 (Fig. 4D). Since phosphorylation of p53 at Ser 15 and 20 has been reported to play an important role in apoptosis induced by DNA damage [18], our results suggest that edaravone specifically stimulates DNA damage-induced apoptosis signaling. On the other hand, the accumulation of p53 and its phosphorylation at Ser 6, Ser 9, and Ser 392 induced by X-irradiation did not increase significantly in the presence of edaravone (Fig. 4D).

Since edaravone enhances DNA damage-induced apoptosis, we next investigated the expression of p53 target genes, especially an apoptosis-related protein PUMA, which is a pro-apoptotic Bcl-2 family protein and induced by DNA damage [8,19]. The expression of PUMA was apparent 4 h after 2 Gy X-irradiation, and it increased significantly when a low dose of edaravone was added before X-irradiation (Fig. 4E). On the other hand, the expression of PUMA induced by X-irradiation was suppressed in the presence of 3 mg/ml edaravone (Fig. 4E), which is compatible with its radioprotective effect shown previously for that dose [3]. The expression of PUMA in the p53 knock-down transformants was not as apparent as that in wild-type MOLT-4 cells after X-irradiation in the presence or absence of edaravone (Fig. 4B). The results indicate that the low dose of edaravone enhanced the expression of the p53 target gene PUMA, and suggest that the enhanced expression contributed to the promotion of apoptosis.

4. Discussion

We found that a low dose of edaravone enhanced X-ray-induced cell death (Fig. 1A–C). This radiosensitizing effect was observed in multiple p53 wild-type cell lines (Figs.

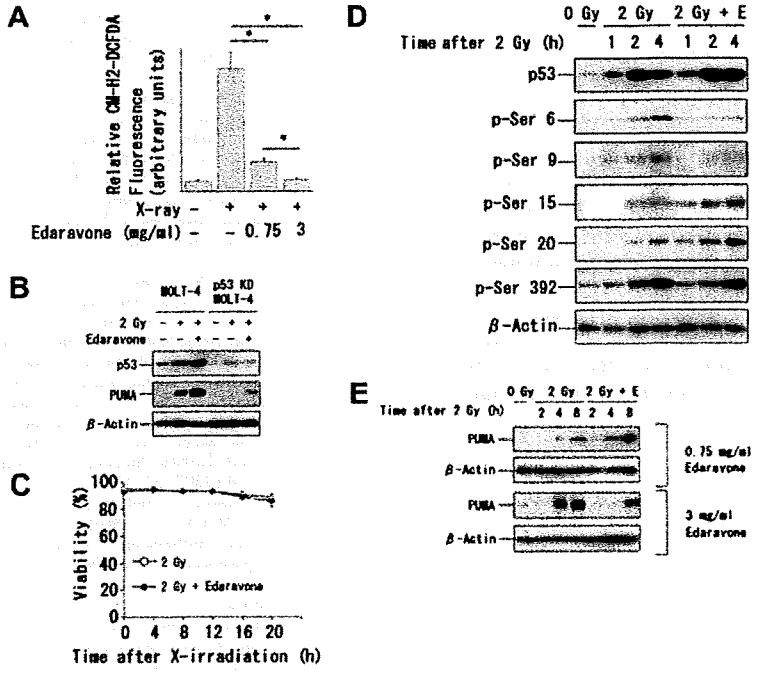

Fig. 4. p53 is involved in the radiosensitizing effect of low dose of edaravone. (A) Intracellular ROS determined by the CM-H_2-DCFDA flow cytometry system. The amount of intracellular ROS after treatment (20 Gy X-irradiation with or without 0.75 or 3 mg/ml edaravone) is shown. Edaravone was added 5 min before X-irradiation. The ROS production of each sample was quantified as described in Materials and methods. Data shown are means ± SD from at least three independent experiments. *$P < 0.05$. (B) MOLT-4 cells and its stable transformants (p53 knock-down (KD) MOLT-4 cells) were X-irradiated with or without 0.75 mg/ml edaravone, then subjected to Western blot analysis with p53 or PUMA antibody. β-Actin is used as a loading control. (C) MOLT-4 and p53 knock-down MOLT-4 cells were X-irradiated with 0.75 mg/ml edaravone, and harvested for the indicated times. (D) Effects of the low dose of edaravone (E) on X-ray-induced accumulation or phosphorylations of p53 at Ser 6, Ser 9, Ser 15, Ser 20, or Ser 392. β-Actin was used as a loading control. (E) Effects of edaravone on X-ray-induced induction of p53 targets, PUMA. MOLT-4 cells were X-irradiated in the absence or presence of the indicated concentrations of edaravone, and harvested at the indicated times. β-Actin was used as a loading control.

Please cite this article in press as: N. Sasano et al., Edaravone, a known free radical scavenger, enhances X-ray-induced apoptosis at low concentrations, Cancer Lett. (2010), doi:10.1016/j.canlet.2009.12.020

1A–C, 2A and B), but not in p53 knock-down MOLT-4 (Fig. 4C). The radiosensitization was mainly caused by enhancing apoptosis (Fig. 3A–D), although ROS was partially suppressed (Fig. 4A), indicating that the radiosensitizing effect was not due to enhancement of ROS generation. We next investigated whether DNA damage signaling pathways were up-regulated, especially the p53-dependent pathway. Although p53 accumulation did not change after X-irradiation in the absence or presence of edaravone, the phosphorylation of p53 at Ser 15 and Ser 20 was enhanced by adding edaravone before X-irradiation (Fig. 4D). Moreover, up-regulation of the p53 target gene, PUMA, was observed with the addition of a low dose of edaravone (Fig. 4E).

PUMA has been reported to play a causal role in p53-dependent apoptosis. Villunger et al. [8] demonstrated that DNA damage-induced apoptosis decreased in PUMA-disrupted mouse fibroblasts and loss of PUMA protected lymphocytes from cell death. The expression of PUMA, which is induced by p53, might contribute to the radiosensitizing effect of edaravone. Our results suggest that the enhancement of phosphorylations of p53 alter the expression pattern of the p53 target genes, causing the promotion of apoptosis.

A question which remains to be answered is why a low dose of edaravone enhances X-ray-induced apoptosis even though it partially eliminates the intracellular ROS generated by X-irradiation (Fig. 4A). In the previous study, a higher dose (3 mg/ml) of edaravone completely eliminated intracellular ROS generated by X-irradiation, causing the suppression of p53 accumulation and phosphorylation at Ser15 [3]. In the present study, p53 phosphorylation at Ser 15 and Ser 20 were enhanced in the presence of edaravone after X-irradiation. The phosphorylation of p53 at Ser 15 or Ser 20 has been shown to be mediated by the ATM, leading to p53 activation [20]. A low dose of edaravone might effect on the activity of ATM or the related protein kinases, resulting in the enhanced phosphorylation of p53, at least at Ser 15 and Ser 20.

We conclude that a low dose of edaravone (0.75 mg/ml) used in this study enhanced X-ray-induced apoptosis by modifying p53 transcriptional activity. The results of the current study may have important clinical implications for radiation therapy.

5. Conflicts of Interest

None declared.

Acknowledgements

We thank all the members of our laboratory for their help and encouragement. We also thank Dr. T. Kondo (University of Toyama) for various suggestions and instructions. This study was supported in part by the Mitsubishi Tanabe Pharma Corporation (Tokyo, Japan). This study was also supported in part by the Radiation Effects Association.

References

[1] Edaravone Acute Infarction Study Group, Effect of a novel free radical scavenger edaravone (MCI-186) on acute brain infarction. Randomized placebo-controlled double-blind study at multicenters, Cerebrovasc. Dis. 15 (2003) 222–229.
[2] S. Abe, K. Kirima, K. Tsuchiya, M. Okamoto, T. Hasegawa, H. Houchi, M. Yoshizumi, T. Tamaki, The reaction rate of edaravone (3-methyl-1-phenyl-2-pyrazolin-5-one (MCI-186)) with hydroxyl radical, Chem. Pharm. Bull. (Tokyo) 52 (2004) 186–191.
[3] N. Sasano, A. Enomoto, Y. Hosoi, Y. Katsumura, Y. Matsumoto, K. Shiraishi, K. Miyagawa, H. Igaki, K. Nakagawa, Free radical scavenger edaravone suppresses X-ray-induced apoptosis through p53 inhibition in MOLT-4 cells, J. Radiat. Res. (Tokyo) 48 (2007) 495–503.
[4] A. Enomoto, N. Suzuki, Y. Kang, K. Hirano, Y. Matsumoto, J. Zhu, A. Morita, Y. Hosoi, K. Sakai, H. Koyama, Decreased c-Myc expression and its involvement in X-ray-induced apoptotic cell death of human T-cell leukemia cell line MOLT-4, Int. J. Radiat. Biol. 79 (2003) 589–600.
[5] G.M. Wahl, A.M. Carr, The evolution of diverse biological responses to DNA damage: insights from yeast and p53, Nature Cell Biol. 3 (2001) E277–E286.
[6] J.R. Jeffers, E. Parganas, Y. Lee, C. Yang, J. Wang, J. Brennan, K.H. MacLean, J. Han, J.N. Ihle, P.J. McKinnon, J.L. Cleveland, G.P. Zambetti, Puma is an essential mediator of p53-dependent and- independent apoptotic pathways, Cancer Cell 4 (2003) 321–328.
[7] K. Nakano, K.H. Vousden, PUMA a novel proapoptotic gene is induced by p53, Mol. Cell 7 (2001) 683–694.
[8] A. Villunger, E.M. Michalak, L. Coultas, F. Müllauer, G. Böck, M.J. Ausserlechner, J.M. Adams, A. Strasser, p53- and drug-induced apoptotic responses mediated by BH3-only proteins puma and noxa, Science 302 (2003) 1036–1038.
[9] J. Yu, Z. Wang, K.W. Kinzler, B. Vogelstein, L. Zhang, PUMA mediates the apoptotic response to p53 in colorectal cancer cells, Proc. Natl. Acad. Sci. USA 100 (2003) 1931–1936.
[10] H. Nakano, M. Kohara, K. Shinohara, Evaluation of the relative contribution of p53-mediated pathway in X-ray-induced apoptosis in human leukemic MOLT-4 cells by transfection with a mutant p53 gene at different expression levels, Cell Tissue Res. 306 (2001) 101–106.
[11] K.E. Rosenzweig, M.B. Youmell, S.T. Palayoor, B.D. Price, Radiosensitization of human tumor cells by the phosphatidylinositol 3-kinase inhibitors wortmannin and LY294002 correlates with inhibition of DNA-dependent protein kinase and prolonged G2-M delay, Clin. Cancer Res. 3 (1997) 1149–1156.
[12] J.N. Sarkaria, R.S. Tibbetts, E.C. Busby, A.P. Kennedy, D.E. Hill, R.T. Abraham, Inhibition of phosphoinositide 3-kinase related kinases by the radiosensitizing agent wortmannin, Cancer Res. 58 (1998) 4375–4382.
[13] M. Tomita, N. Suzuki, Y. Matsumoto, A. Enomoto, H.L. Yin, Y. Hosoi, K. Hirano, K. Sakai, Wortmannin-enhanced X-ray-induced apoptosis of human T-cell leukemia MOLT-4 cells possibly through the JNK/SAPK pathway, Radiat. Res. 160 (2003) 467–477.
[14] H. Shibata, S. Arai, M. Izawa, M. Murasaki, Y. Takamatsu, O. Izawa, C. Takahashi, M. Tanaka, Phase I clinical study of MCI-186 (Edaravone; 3-methyl-1-phenyl-2-pyrazolin-5-one) in healthy volunteers: safety and pharmacokinetics of single and multiple administration, Jpn. J. Clin. Pharmacol. Ther. 29 (1998) 863–876.
[15] S. Kumar, Caspase function in programmed cell death, Cell Death Differ. 14 (2007) 32–43.
[16] T. Nishikawa, D. Edelstein, X. Du, S. Yamagishi, T. Matsumura, Y. Kaneda, M.A. Yorek, D. Beebe, P.J. Oates, H.P. Hammes, I. Giardino, M. Brownlee, Normalizing mitochondrial superoxide production blocks three pathways of hyperglycaemic damage, Nature 404 (2000) 787–790.
[17] A. Morita, J. Zhu, N. Suzuki, A. Enomoto, Y. Matsumoto, M. Tomita, T. Suzuki, K. Ohtomo, Y. Hosoi, Sodium orthovanadate suppresses DNA damage-induced caspase activation and apoptosis by inactivating p53, Cell Death Differ. 13 (2006) 499–511.
[18] E. Appella, C.W. Anderson, Post-translational modifications and activation of p53 by genotoxic stresses, Eur. J. Biochem. 268 (2001) 2764–2772.
[19] X. Wu, Y. Deng, Bax and BH3-domain-only proteins in p53-mediated apoptosis, Front. Biosci. 7 (2002) d151–d156.
[20] G.A. Turenne, P. Paul, L. Laflair, B.D. Price, Activation of p53 transcriptional activity requires ATM's kinase domain and multiple N-terminal serine residues of p53, Oncogene 20 (2001) 5100–5110.

Please cite this article in press as: N. Sasano et al., Edaravone, a known free radical scavenger, enhances X-ray-induced apoptosis at low concentrations, Cancer Lett. (2010), doi:10.1016/j.canlet.2009.12.020

Vascular Endothelial Growth Factor C Stimulates Progression of Human Gastric Cancer via Both Autocrine and Paracrine Mechanisms

Michiyo Kodama,[1] Yasuhiko Kitadai,[1] Miwako Tanaka,[1] Toshio Kuwai,[3] Shinji Tanaka,[4] Naohide Oue,[2] Wataru Yasui,[2] and Kazuaki Chayama[1]

Abstract

Purpose: Vascular endothelial growth factor (VEGF)-C induces lymphangiogenesis by activating the VEGF receptor (VEGFR)-3, which is expressed by lymphatic endothelial cells. VEGFR-3 has also been detected on several malignant cells, but the significance of VEGFR-3 expression on malignant cells remains unclear. In this study, we examined the expression and function of VEGFR-3 in gastric carcinoma cells.

Experimental Design: We examined the expression of VEGFR-3 by four human gastric carcinoma cell lines and in 36 surgical specimens of gastric carcinoma. We also used cDNA microarrays to examine the effect of VEGF-C on gene expression in VEGFR-3-expressing KKLS cells. To stimulate VEGF-C/VEGFR-3 signaling in an autocrine manner, the VEGF-C expression vector was transfected into KKLS cells, and stable transfectants were established. These cells were then transplanted into the gastric walls of nude mice.

Results: Two of the four gastric carcinoma cell lines expressed *VEGFR-3* mRNA. In 17 of 36 gastric carcinoma specimens, VEGFR-3-specific immunoreactivity was detected on tumor cells. *In vitro* treatment of KKLS cells with VEGF-C stimulated cell proliferation and increased expression of mRNAs encoding cyclin D1, placental growth factor, and autocrine motility factor. Following inoculation of VEGF-C-transfected and control cells into the gastric walls of nude mice, tumor growth of the VEGF-C-transfected cells was greatly accelerated in comparison with that of control cells. Greater angiogenesis and lymphangiogenesis were also detected in VEGF-C-transfected tumors than in control tumors.

Conclusions: Gastric carcinoma cells express VEGF-C and VEGFR-3. VEGF-C may play a role in the progressive growth of human gastric carcinoma through both autocrine and paracrine mechanisms.

The process of cancer metastasis is sequential and selective and consists of a series of interlinked independent steps (1). To produce a metastatic lesion, tumor cells must complete all of the steps, which include angiogenesis, motility, invasion, survival in the circulation, adhesion, extravasation, and proliferation (2, 3). Several sets of growth factors and their cognate receptors have been reported to be important in the regulation of metastasis. For example, cancer cells attach to the vascular endothelium via adhesion molecules, invade the tissue via motility factors, grow in the tissue with the help of growth factors, and establish their blood supply by the participation of angiogenic factors. Thus, disruption of a growth factor/receptor axis is a current strategy for the development of anticancer drugs (4).

The vascular endothelial growth factor (VEGF) family includes VEGF-A, VEGF-B, VEGF-C, VEGF-D, VEGF-E, and placental growth factor (PlGF; refs. 5, 6). The importance of VEGF and VEGF receptor (VEGFR) expression in tumor angiogenesis and lymphangiogenesis is supported by several lines of evidence. VEGF-A is one of the most potent stimulators of angiogenesis identified thus far, affecting endothelial cell proliferation and motility and vascular permeability (7). VEGF-A exerts its angiogenic functions through activation of the tyrosine kinase receptors VEGFR-1 (Flt-1) and VEGFR-2 (Flk-1/KDR), which are expressed primarily by vascular endothelial cells (8). However, VEGFRs are also expressed by a wide variety of cancer cell lines. VEGF-A and VEGFR-1/2 are coexpressed in a number of cancers, including cancers of the breast (9), prostate (10), colon (11), and pancreas (12, 13), suggesting that VEGF-A may directly influence tumor cell growth via an autocrine mechanism.

VEGF-C induces lymphangiogenesis by activating VEGFR-3, which is expressed by lymphatic endothelial cells (14). We

Authors' Affiliations: Departments of [1]Medicine and Molecular Science and [2]Pathology, Graduate School of Biomedical Sciences, Hiroshima University; [3]Department of Internal Medicine, National Hospital Organization Kure Medical Center; and [4]Department of Endoscopy, Hiroshima University Hospital, Hiroshima, Japan

Received 4/3/08; revised 7/24/08; accepted 8/4/08.

Grant support: Grants-in-Aid for Cancer Research from the Ministry of Education, Culture, Science, Sports and Technology of Japan; and from the Ministry of Health, Labor and Welfare of Japan.

The costs of publication of this article were defrayed in part by the payment of page charges. This article must therefore be hereby marked *advertisement* in accordance with 18 U.S.C. Section 1734 solely to indicate this fact.

Requests for reprints: Yasuhiko Kitadai, Hiroshima University Graduate School of Biomedical Sciences, 1-2-3 Kasumi, Minami-ku, Hiroshima 734-8551, Japan. Phone: 81-82-257-5193; Fax: 81-82-257-5194; E-mail: kitadai@hiroshima-u.ac.jp.

doi:10.1158/1078-0432.CCR-08-0818

Translational Relevance

Many studies in experimental models of cancer have shown that the vascular endothelial growth factor (VEGF)-C/VEGF receptor-3 (VEGFR-3) signaling system is a key regulator of tumor lymphangiogenesis. In the present study, we showed that tumor cells express not only VEGF-C but also VEGFR-3 in human gastric carcinoma. *In vitro* and *in vivo* experiments showed VEGF-C acts as a growth factor for carcinoma cells, in addition to acting as a lymphangiogenic or angiogenic factor. Therefore, VEGF-C may play a role in the progressive growth of human gastric carcinoma through both autocrine and paracrine mechanisms. We propose that interruption of the VEGF-C/VEGFR-3 axis may be a therapeutic approach for controlling disease progression. Reagents that block this pathway could provide benefit for patients with gastric carcinoma in the clinic.

reported previously that expression of VEGF-C correlates with lymph node metastasis in several malignancies, including esophageal (15), gastric (16), and colorectal (17) carcinomas. VEGFR-3 has also been detected on malignant cells, including lung adenocarcinoma (18), head and neck carcinomas (19), prostate carcinoma (20), and leukemia cells (21). These observations suggest that VEGF-C may directly affect cancer cells. Su et al. (18) reported that the VEGF-C/VEGFR-3 axis plays an important role in promoting invasion and metastasis of human lung adenocarcinoma cells. However, unlike the well-characterized axes of VEGF-A and VEGFR-1/2, the biological significance of the activation of the VEGF-C/VEGFR-3 axis in epithelial tumor cells is not well understood. The expression status and significance of VEGFR-3 on gastric carcinoma cells remain unclear. In the present study, to characterize the VEGF-C/VEGFR-3 axis in gastric carcinoma, we examined the expression and function of VEGFR-3 on gastric carcinoma cell lines and tissue specimens.

Materials and Methods

Patients and tumor specimens. Thirty-six patients who underwent surgical resection for gastric carcinoma without preoperative treatment at Hiroshima University Hospital, Hiroshima, Japan, were enrolled in this study. The patient group comprised 32 men and 4 women; median age was 66 y. Informed consent was obtained from all patients for participation in the study. Paraffin-embedded archival specimens from the patients were examined by immunohistochemistry. Pathology reports and clinical histories were reviewed for accurate staging at the time of surgery. Criteria for staging and histologic classification were those proposed by the Japanese Research Society for Gastric Cancer (22). All patients had invasive gastric carcinoma in which the tumor invasion was beyond the submucosa (21 patients stage II; 15 patients stage III).

Cell cultures. Four cell lines established from human gastric carcinomas were maintained in RPMI 1640 (Nissui Co.) with 10% fetal bovine serum (FBS; MA BioProducts). The TMK-1 cell line (a poorly differentiated adenocarcinoma) was provided by Dr. E. Tahara of Hiroshima University. The KKLS cell line (an undifferentiated carcinoma) was provided by Dr. Y. Takahashi of Chiba University, Chiba, Japan. The other two cell lines (MKN-1, from an adenosquamous carcinoma, and MKN-28, from a well-differentiated adenocarcinoma) were obtained from the Health Science Research Resources Bank, Osaka, Japan.

Cell proliferation assays. *In vitro* growth was measured with a Cell Proliferation Biotrak ELISA System, version 2 (Amersham Biosciences), according to the manufacturer's instructions to determine whether recombinant human VEGF-C (rhVEGF-C; R&D Systems) would stimulate proliferation of KKLS cells. Cells were seeded in a 96-well plate at a density of 1×10^4 cells per well and incubated overnight in 200 μL culture medium containing 10% FBS. After incubation for 24 h, cells were cultured in serum-free culture medium containing 10 μmol/L bromodeoxyuridine with or without rhVEGF-C for 24 h, and cell proliferation was measured in a plate reader (Microplate Manager 5.2.1; Bio-Rad) at 450 nm.

Microarray analysis. KKLS cells were cultured in RPMI 1640 without FBS for 6 h and then cultured with or without rhVEGF-C (20 ng/mL) for 8 h. These cells were collected and stored at -80°C until use. Microarray analysis was done with the Human Cancer CHIP (version 4, Takara Shuzo), which contains 637 human cancer-related genes (listed on the home page of Takara Shuzo[5]) spotted on glass plates. A fluorescent probe synthesized by reverse transcription of 1 μg of the above mRNA with 50 U AMV reverse transcriptase (Takara Shuzo) was added to each reaction mixture. Cy3- and Cy5-labeled probes were prepared from mRNAs isolated from control cells and rhVEGF-C-treated cells, respectively; both were mixed in the reaction buffer [6× SSC, 0.2% SDS, 5× Denhardt's solution, 0.8 mg/mL poly(dA), and 1 mg/mL yeast tRNA]. The mixture was hybridized to the cDNA CHIP at 65°C overnight. The CHIP was washed twice with 2× SSC/0.2% SDS solution at 55°C for 30 min and then with the same solution at 65°C for 5 min. Finally, the CHIP was washed with 0.05× SSC at room temperature for 10 min. Signals on the hybridized CHIP were visualized and quantified with the Scan-Array 5000 (GSI Lomonids) and normalized to the averaged signals of housekeeping genes. Genes were excluded from further investigation when the intensities of both Cy3 and Cy5 were below 1,000 fluorescence units. Those with Cy3/Cy5 signal ratios >2.0 were regarded as up-regulated.

Semiquantitative and quantitative reverse transcription-PCR. Total RNA was extracted from gastric carcinoma cell lines with an RNeasy Kit (Qiagen) according to the manufacturer's instructions. cDNA was synthesized from 1 μg total RNA with a first-strand cDNA synthesis kit (Amersham Biosciences). After reverse transcription of RNA into cDNA, quantitative reverse transcription-PCR (RT-PCR) was done with a LightCycler-FastStart DNA Master SYBR-Green I Kit (Roche), and semiquantitative RT-PCR was done with an AmpliTaq Gold Kit (Roche) according to the manufacturer's recommendations. Quantitative RT-PCR was used to monitor gene expression and was done with a LightCycler system and LightCycler Data Analysis Software ver. 3.5 (Roche) in accordance with standard procedures. PCR reactions were carried out in triplicates. To correct for differences in both RNA quality and quantity between samples, the data were normalized to those of *β-actin*. Primers for PCR were designed with specific primer analysis software (Primer Designer, Scientific and Educational Software), and the specificity of the sequences was confirmed by FASTA (EMBL Database). Primer sequences, annealing temperatures (Ta), and PCR cycles were as follows: VEGF-C forward, GAGGAGCAGTTACGGTCTGT and VEGF-C reverse, GTAGCTCGTGCTGGTGTTCA (*VEGF-C* PCR product, 371 bp; Ta, 59°C; 28 cycles); VEGFR-3 forward, GGTTCCTCCAGGATGAAGAC and VEGFR-3 reverse, CAAGCAGTAACGCCAGTGTC (*VEGFR-3* PCR product, 505 bp; Ta, 62°C; 28 cycles); AMFR forward, ACTCTCCTGTCCCTGGACCT and FLT-4 reverse, TCATTGTTGACAGCCAGCTC (*AMFR* PCR product, 218 bp; Ta, 59°C; 35 cycles); AMF forward, CGCCCAACCAACTCTATTGT and AMF reverse, GGTAGAAGCGTCGTGAGAGG (*AMF* PCR product, 213 bp; Ta, 59°C; 40 cycles); PlGF forward, ATGTTCAGCCCATCCTGTGT and

[5] http://bio.takara.co.jp/catalog/DNAChip.Down-load.htm

PlGF reverse, CTTCATCTTCTCCCGCAGAG (*PlGF* PCR product, 201 bp; Ta, 59°C; 40 cycles); GAPDH forward, ATCATCCCTGCCTCTACTGG and GAPDH reverse, CCCTCCGACGCCTGCTTCAC (*GAPDH* PCR product, 188 bp; Ta, 55°C; 28 cycles); and β-actin forward, GGACTTCGAGCAAGAGATGG and β-actin reverse, AGCACTGTGTTGGCGTACAG (*β-actin* PCR product, 234 bp; Ta, 55°C;35 cycles). After amplification, PCR products were resolved on 5% nondenaturing polyacrylamide gels in Tris-borate-EDTA buffer. RT-PCR in the absence of reverse transcriptase showed no specific bands.

Immunohistochemical staining. Immunohistochemistry for VEGF-C, VEGFR-3, Lyve1, and Ki-67 was done on formalin-fixed, paraffin-embedded tissues cut into serial 4-μm sections. After deparaffinization and rehydration, tissue sections for staining of VEGF-C and VEGFR-3 were pretreated by microwave twice for 5 min in Dako REAL Target Retrieval Solution (Dako). Immunohistochemical staining of CD31 was done on fresh-frozen specimens cut into 8-μm sections, mounted on positively charged slides and stored at -80°C. Frozen tissue sections were fixed in cold acetone for 10 min. VEGF-C was detected with a goat antihuman polyclonal antibody (1:200; R&D Systems), and VEGFR-3 was detected with a goat antihuman polyclonal antibody (1:50; R&D Systems). Lyve1 was detected with the rat antimouse monoclonal antibody (1:20; R&D Systems), and Ki-67 was detected with the mouse antihuman polyclonal antibody (MIB-1; 1:25, Dako). CD31 was detected with the rat antimouse polyclonal antibody (1:200; Pharmingen). The primary antibodies were applied to the slides and incubated overnight in humidified boxes at 4°C. After incubation for 1 h at room temperature with peroxidase-conjugated corresponding secondary antibodies, a positive reaction was detected by exposure for 5 to 10 min to stable 3,3′-diaminobenzidine. Slides were counterstained with hematoxylin for visualization of the nucleus.

Gene transfection and cloning of transfected cell lines. A full-length *VEGF-C* cDNA (a 1.9-kbp *Eco*RI-*Eco*RI fragment) was inserted into the *Eco*RI-*Eco*RI site of pBR322 (Invitrogen). The resultant plasmid was digested with *Xho*I-*Bam*HI and cloned into the *Xho*I-*Bam*HI site of the pEGFP-N1 expression vector (BD Biosciences) to yield the *VEGF-C* expression vector. Expression of *VEGF-C* cDNA was under the control of the cytomegalovirus promoter. The KKLS cell line was transfected with either the *VEGF-C* expression vector or the pEGFP-N1 vector alone with Lipofectin (Life Technologies) according to the manufacturer's instructions. After transfection, cells were grown in selective medium (10% FBS-RPMI 1640 containing 800 μg/mL G418). The selective medium was changed every 3 d. G418-resistant clones (KKLS/VEGF-C and KKLS/EGFP) were selected and then expanded for additional studies. G418 was from Sigma.

ELISA for VEGF-C protein. For generation of conditioned media, tumor cells were plated at 1.0×10^5/mL per 10-cm dish (Becton Dickinson Labware), and the supernatants were collected after 48 h, centrifuged to remove floating cells, and stored at -80°C. We used the Quantikine Human VEGF-C Immunoassay (R&D Systems) according to the manufacturer's instructions to measure VEGF-C levels.

Western blot analysis. Expression of VEGF-C, VEGFR-3, and cyclin D1 was evaluated by Western blot analysis. The phosphorylation status of VEGFR-3 or Akt was also evaluated by Western blot analysis. To evaluate VEGFR-3 or Akt phosphorylation of KKLS cells stimulated with VEGF-C, cells were seeded in 10-cm dishes (1.5×10^5 cells per dish) in growth medium and allowed to attach overnight before the growth medium was replaced with serum-free medium for an additional 24-h incubation. The cells were then stimulated with or without VEGF-C (20 ng/mL) for 5 or 10 min at 37°C. To evaluate VEGFR-3 or Akt phosphorylation in KKLS cells transfected with expression vector, cells

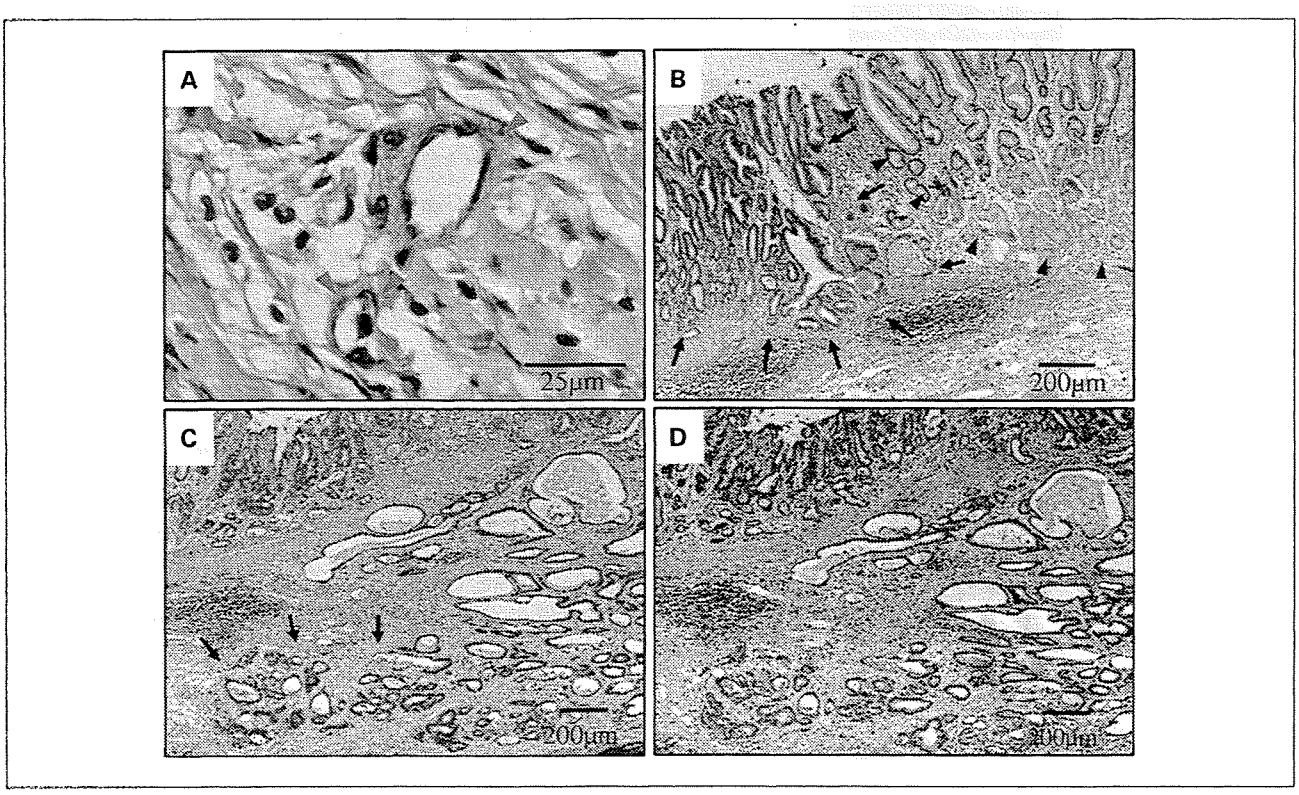

Fig. 1. Expression of VEGFR-3 and VEGF-C in human gastric carcinoma tissues. Immunoreactivity of VEGFR-3 was detected on tumor cells in 17 of 36 (47.2%) gastric carcinoma specimens. *A*, staining of VEGFR-3 on lymphatic vessels (*red arrowhead*). *B*, homogeneous staining of VEGFR-3 (*black arrow*) was observed in 7 of 17 specimens. Normal mucosa did not show VEGFR-3 staining (*black arrowhead*). *C*, in 10 of 17 specimens, VEGFR-3 expression was heterogeneous. Immunoreactivity for VEGFR-3 was more intense at the deepest invasive site (*black arrow*) than at the central portion or superficial part. *D*, VEGF-C immunoreactivity was detected on tumor cells.

were seeded in 10-cm dishes (1.5×10^5 cells per dish) in growth medium and allowed to attach overnight before the growth medium was replaced by serum-free medium for an additional 24-h incubation. After three washes with cold PBS containing 1 mmol/L sodium orthovanadate, cells were lysed. Protein samples of the cell lysates (total protein 20 μg) or 1 μL of culture medium were separated by SDS-PAGE and transferred to nitrocellulose transfer membranes (Whatman GmbH). After being blocked with 1% or 3% skim milk in TBS, the membranes were incubated with primary antibodies, namely, polyclonal goat antihuman VEGF-C antibody, polyclonal goat antihuman VEGFR-3 antibody, polyclonal mouse antihuman cyclin D1 (Dako), polyclonal rabbit antihuman phopho-VEGFR-3 antibody (Calbiochem), polyclonal rabbit antibody to phospho-Akt (phosphorylated at Ser473, Cell Signaling Technology), or β-actin (Sigma), and were diluted in TBS at 4°C overnight. The membranes were then washed in TBS-T (0.1% Tween 20 in TBS) and incubated with the secondary antibodies specific for each primary antibody at room temperature for 1 h. To confirm equivalent protein loading, membranes were stripped and reprobed with anti-Akt antibody (Cell Signaling Technology). The immune complexes were visualized with enhanced chemiluminescence with an ECL Plus Kit (Amersham Life Science).

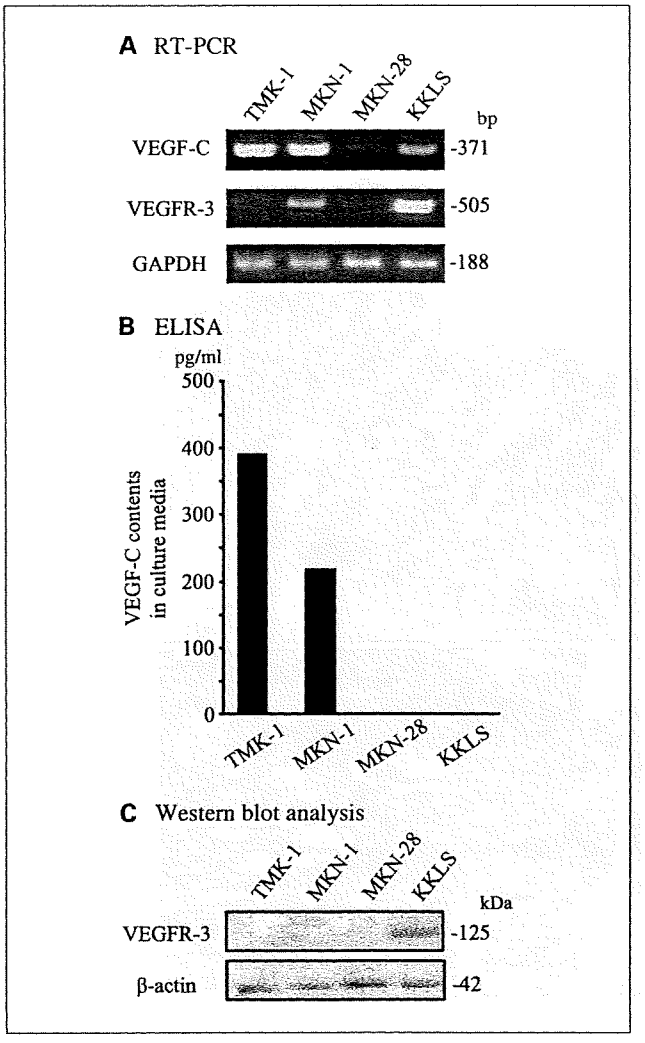

Fig. 2. Expression of VEGF-C and VEGFR-3 in gastric carcinoma cell lines. *A, VEGF-C* and *VEGFR-3* expression by gastric cell lines was examined by RT-PCR. *B,* culture supernatants were assayed for VEGF-C by ELISA. *C,* VEGFR-3 protein expression was analyzed by Western blotting.

Immunofluorescence staining for pVEGFR-3. To confirm the activation of VEGFR-3 by VEGF-C, KKLS cells were cultured in RPMI 1640 without FBS for 24 h and then stimulated with or without rhVEGF-C (20 ng/mL) for 10 min. Tumor cells were stained with pVEGFR-2, 3 (1:1,000; Calbiochem).

Animal models. Male athymic BALB/c nude mice were obtained from Charles River Japan. The mice were maintained under specific pathogen-free conditions and used at 5 wk of age. This study was carried out after permission was granted by the Committee on Animal Experimentation of Hiroshima University.

Orthotopic (gastric mucosa) xenograft model. For implantation, subconfluent KKLS/VEGF-C and KKLS/EGFP cells were harvested by brief treatment with 0.25% trypsin and 0.02% ethylenediamine tetraacetic acid, and resuspended to a final concentration of 2.0×10^7 cells/mL Hanks' solution. Using a 30-gauge needle attached to a 1-mL syringe, cells (1.0×10^6/0.05 mL) were implanted into the gastric walls of nude mice under observation with a zoom stereomicroscope. After 4 wk, the mice were sacrificed, and the tumors were resected for study. The tumors were fixed in 10% buffered formalin or formalin-free IHC Zinc Fixative (Pharmingen) for immunohistochemistry.

Quantitation of lymphatic vessel density, microvessel density, and Ki-67 labeling index. Lymphatic vessel density and microvessel density were determined from counts of Lyve1-positive vessels and CD31-positive vessels, respectively. Vessel counts were assessed by light microscopy in immunohistochemistry-stained areas of the intratumoral and peritumoral regions containing the highest numbers of capillaries and small venules (23). Highly vascularized areas were first identified by scanning tumor sections at low power (×40 and ×100). The vessel count was determined for six such areas at ×400 (×40 objective and ×10 ocular), and the mean of the six counts was calculated. A vessel lumen was not necessary for a structure to be defined as a blood microvessel (23). In slides immunolabeled for Lyve1, only vessels with typical morphology (including a lumen) were counted as lymphatic vessels because of occasional weak antibody cross-reactivity with fibroblasts (24). The Ki-67 labeling index was determined by light microscopy at the site of the greatest number of Ki-67–positive cells. The sites were identified by scanning tumor sections at low power (×40). For the Ki-67 labeling index, the number of positive cells among ~1,000 tumor cells was calculated as a percentage. Staining of cells was evaluated by two independent observers (M.K. and Y.K.) blinded to the patient's status.

Statistical analysis. Results are expressed as mean ± SE. Fischer's exact test or χ^2 test was used for the analysis of categorical data. Wilcoxon/Kruskal-Wallis analysis was used for comparison of continuous variables. A P value of <0.05 was considered statistically significant.

Results

Immunolocalization of VEGFR-3 in human gastric carcinoma tissues. We analyzed 36 human gastric cancer specimens with a polyclonal antibody specific for human VEGFR-3. We detected VEGFR-3-specific immunoreactivity on lymphatic endothelial cells (Fig. 1A). In 17 of 36 (47.2%) gastric carcinoma specimens, VEGFR-3-specific immunoreactivity was detected on tumor cells (Fig. 1B and C). Immunoreactivity for VEGFR-3 was more intense at the site of deepest invasion than at the central portion or superficial part of the tumor (Fig. 1C). In 12 of 36 (33.3%) gastric carcinomas, tumor cells expressed both VEGF-C and VEGFR-3 (Fig. 1C and D). VEGFR-3 immunoreactivity was not detected in normal gastric epithelial cells (Fig. 1B).

Expression of VEGF-C and VEGFR-3 in gastric carcinoma cell lines. We next analyzed VEGF-C and VEGFR-3 expression in gastric carcinoma cell lines. Gastric carcinoma cell lines constitutively expressed *VEGF-C* mRNA at various levels. Two

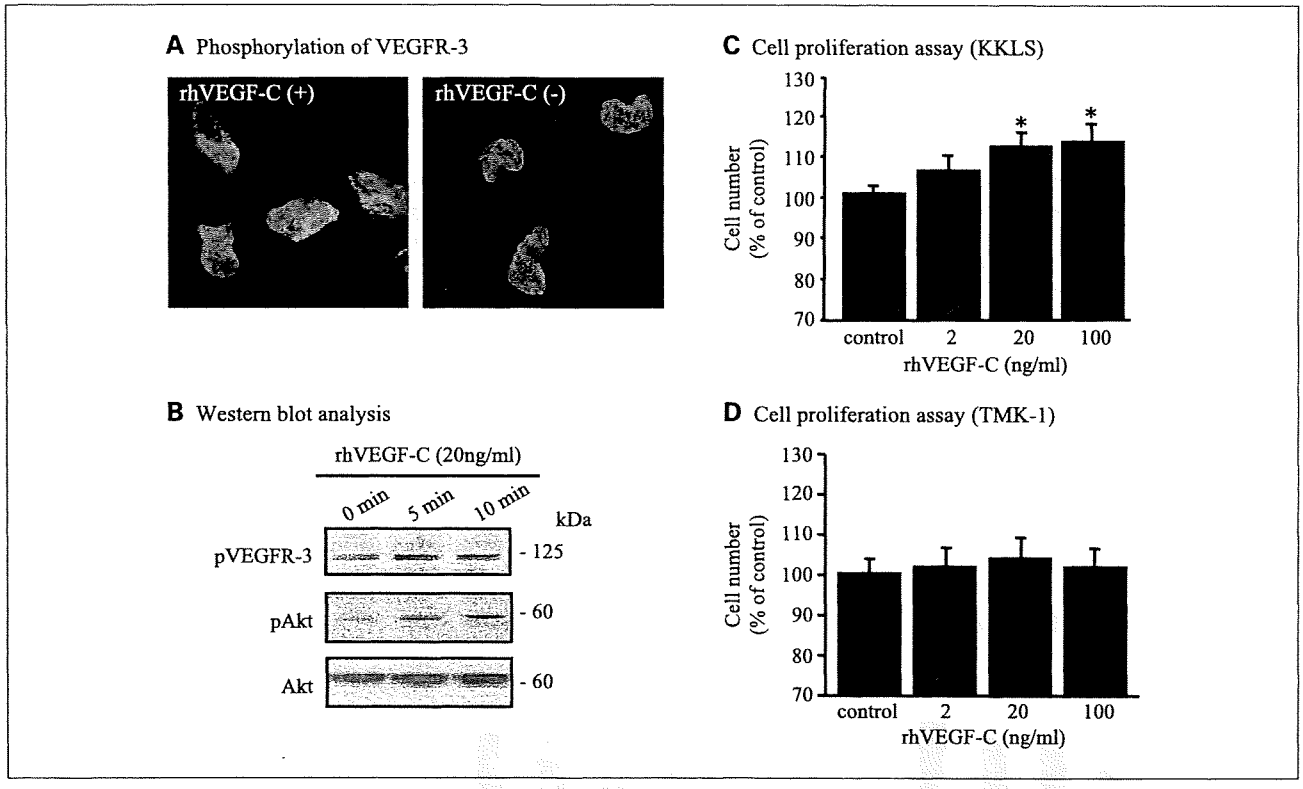

Fig. 3. Effect of VEGF-C on KKLS cells. *A*, VEGF-C-dependent phosphorylation of VEGFR-3. KKLS cells were cultured in medium without FBS for 24 h and then stimulated with or without rhVEGF-C (20 ng/mL) for 10 min. Tumor cells were stained with pVEGFR-2, 3 (*red*). *B*, VEGF-C increases Ser473 phosphorylation of Akt in KKLS cells. KKLS cells were maintained in serum-free medium for 24 h and then treated with 20 ng/mL VEGF-C for the indicated times. Equal amounts of protein (20 μg/lane) were then subjected to Western blot analysis with phospho-specific Akt antibody. Reprobing of the blot with anti-Akt antibody confirmed the equivalent loading of lanes. KKLS (*C*) or TMK-1 (*D*) cells were incubated with rhVEGF-C (2, 20, or 100 ng/mL) for 24 h, and cell proliferation was measured with a cell proliferation ELISA system. Asterisks denote a statistically significant difference compared with control values. * $P < 0.05$; bars, SE.

of the four gastric carcinoma cell lines (KKLS and MKN-1) expressed *VEGFR-3* mRNA. Of these two cell lines, the KKLS cell line overexpressed *VEGFR-3* mRNA (Fig. 2A). Expression of VEGF-C and VEGFR-3 by gastric carcinoma cells was confirmed at the protein level. Culture supernatants were assayed for VEGF-C by ELISA (Fig. 2B). VEGFR-3 protein expression was analyzed by Western blotting (Fig. 2C). KKLS cells expressed high levels of VEGFR-3 protein, but the amount of VEGF-C protein was below the limit of detection, which was not consistent with the level of mRNA. For this reason (high endogenous VEGFR-3 and low endogenous VEGF-C in KKLS cells), we used KKLS cells for further studies.

VEGF-C stimulates proliferation of KKLS cells. To investigate the possibility of autocrine tumor cell growth stimulation by VEGF-C, we treated KKLS cells with rhVEGF-C and analyzed phosphorylation of VEGFR-3, Akt, and mitogen-activated protein kinase in KKLS cells and the effect on cell proliferation. VEGF-C treatment induced phosphorylation of VEGFR-3 and Akt in KKLS cells (Fig. 3A and B) and increased cell proliferation of KKLS cells in a dose-dependent manner (Fig. 3C). Phosphorylation of mitogen-activated protein kinase was not detected (data not shown). In contrast, VEGF-C had no effect on cell proliferation of TMK-1 cells (VEGFR-3 negative cell line; Fig. 3D).

VEGF-C up-regulates expression of genes associated with disease progression in KKLS cells. To study the downstream effector genes of VEGF-C/VEGFR-3 signaling, we did microarray analysis using the Human Cancer CHIP (Takara Shuzo). Expression of various mRNAs in untreated KKLS cells was compared with expression in KKLS cells treated with rhVEGF-C for 8 hours. Under the highly stringent conditions we used, 52 genes were classified as genes showing significantly increased expression in response to VEGF-C. Among these genes, we confirmed the increased expression of cyclin D, PlGF, and autocrine motility factor receptor (AMFR) by quantitative RT-PCR or Western blotting. Treatment with VEGF-C increased expression of *AMFR* mRNA in a dose-dependent and time-dependent manner (Fig. 4A). We also investigated expression of the mRNA encoding AMF, the ligand of AMFR. Treatment with VEGF-C also increased expression of *AMF* mRNA (Fig. 4B). Levels of *PlGF* mRNA were similarly increased in VEGF-C-treated KKLS cells (Fig. 4C). In addition, VEGF-C increased expression of cyclin D1 protein in a dose-dependent manner (Fig. 4D).

Transfection of the VEGF-C gene into KKLS cells. To stimulate autocrine VEGF-C/VEGFR-3 signaling, a *VEGF-C* expression vector was transfected into KKLS cells. After transfection with the VEGF-C expression vector or the control vector (pEGFP-N1), we selected a stable clone (KKLS/VEGF-C) that overexpressed *VEGF-C* and a control clone (KKLS/EGFP) for subsequent assays. Overexpression of *VEGF-C* mRNA and VEGF-C protein was confirmed by quantitative RT-PCR (Fig. 5A) and Western blotting,

respectively (Fig. 5B). Phosphorylation of Akt in KKLS/VEGF-C cells was also confirmed by Western blotting (Fig. 5B).

In vitro *and* in vivo *proliferation of VEGF-C-transfected gastric carcinoma cells.* Under culture conditions of 0.5% FBS, cell proliferation was stimulated by transfection with *VEGF-C* expression vector (Fig. 5C). To investigate the role of the VEGF-C/VEGFR-3 axis in an animal model, we implanted KKLS/VEGF-C and control cells into the gastric walls of nude mice. At the end of the 4-week experimental period, *in vivo* growth of KKLS/VEGF-C cells was significantly greater than that of control cells (Fig. 5D).

We next used immunohistochemistry for Lyve1, CD31, and Ki-67 to investigate lymphatic vessel density, microvessel density, and Ki-67 labeling index. Greater lymphangiogenesis (Fig. 6A) and angiogenesis (Fig. 6B) were observed in mice implanted with VEGF-C-transfected KKLS cells than in those implanted with control KKLS cells. Statistical analysis showed that the number of Ki-67–positive cells, as well as lymphatic vessel density and microvessel density, was significantly higher in the KKLS/VEGF-C tumors than in the control tumors ($P < 0.01$; Fig. 6C).

Discussion

Until recently, studies of VEGF family members have focused primarily on their functions as paracrine stimulators of angiogenesis or lymphangiogenesis. Promotion of tumor metastasis by VEGF-C is reported to be due to the induction of tumor lymphangiogenesis via effects of activated VEGFR-3 on lymphatic endothelial cells (25). Association of VEGF-C with tumor lymphangiogenesis and with lymph node metastasis has been observed in many human carcinomas, including thyroid, prostate, esophageal, gastric, colorectal, and lung cancers (15, 16, 26, 27). Furthermore, several studies have shown that overexpression of VEGF-C induces lymphangiogenesis and promotes tumor metastasis in mouse tumor models (28, 29).

After the discovery of VEGFRs on malignant cells, it was reported that VEGF-A can act as an autocrine growth factor for various types of cancer cells (13, 30, 31). Unlike the well-characterized VEGF-A/VEGFR-2 axis, there may be many undefined functions and molecular mechanisms involved in

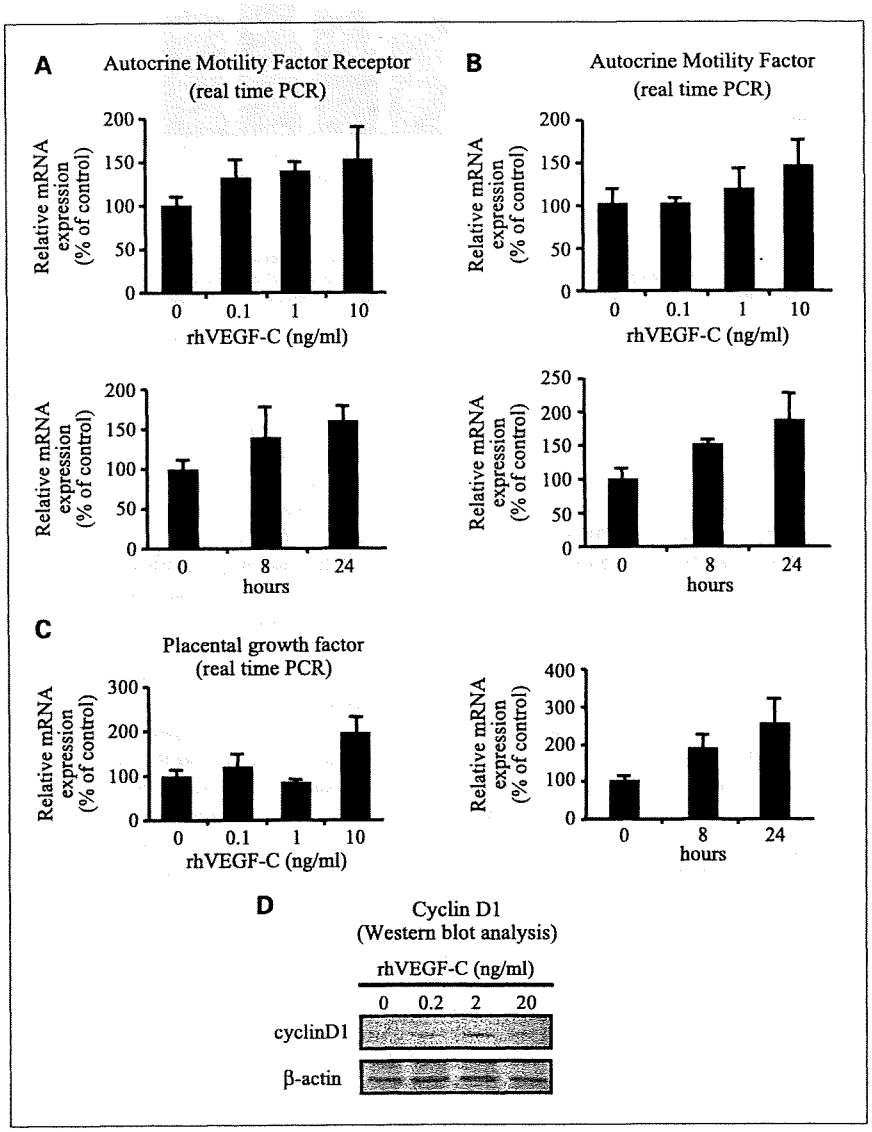

Fig. 4. KKLS cells were treated with various concentrations of rhVEGF-C for 8 h, and the expression of *AMFR* (*A*), *AMF* (*B*), and *PlGF* (*C*) mRNA was determined by RT-PCR. Expression of cyclin D1 protein was examined by Western blot analysis (*D*). PCR reactions were carried out in triplicates. Data for RT-PCR were normalized to those of *β-actin*. Bars, SE.

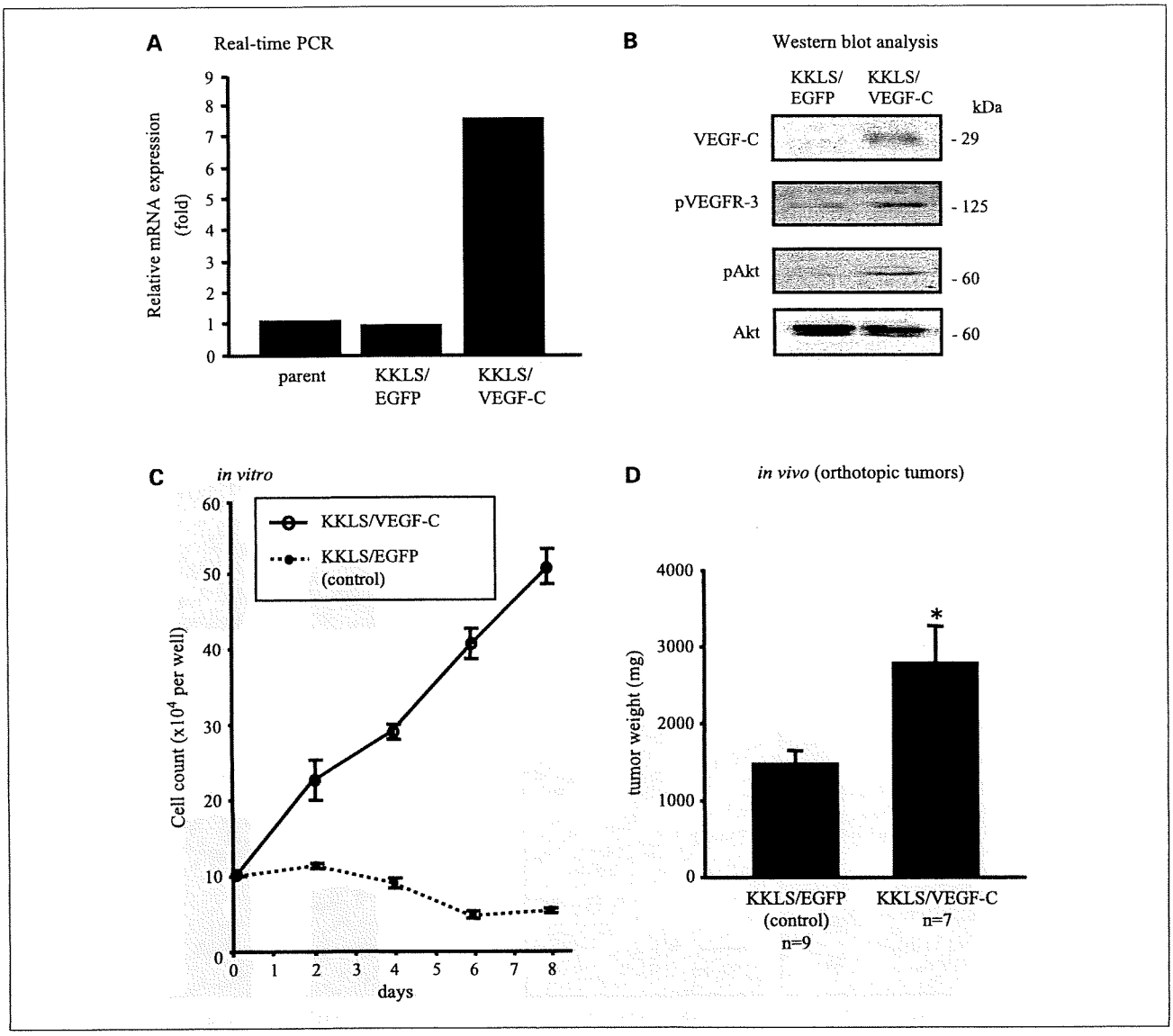

Fig. 5. Establishment of a clonal cell line overexpressing VEGF-C, and *in vitro* and *in vivo* growth of VEGF-C-transfected gastric carcinoma cells. *A*, expression of *VEGF-C* mRNA was examined by RT-PCR. *B*, Western blot analyses of VEGF-C in culture medium of transfected cells and phosphorylation of VEGFR-3 and Akt in lysates of transfected cells. *C*, cells (1×10^5) were seeded in 24-well plates and cultured in medium containing 0.5% FBS. Cell number was determined in triplicate cultures. *D*, orthotopic (gastric mucosa) xenograft model. Tumor weights at 4 wk after implantation of a VEGF-C overexpressing clone (KKLS/VEGF-C) or cells transfected with the corresponding vector control (KKLS/EGFP). * $P < 0.05$; bars, SE.

tumor progression mediated by the VEGF-C/VEGFR-3 axis. Results regarding the expression of VEGFR-3 on tumor cells are controversial. Some studies did not detect expression of VEGFR-3 on tumor cells (32–34), whereas other studies found expression of VEGFR-3 on tumor cells (18–21, 35–37). These contradictory findings suggest that expression of VEGFR-3 on cancer cells may differ between malignancies or cell lines.

Expression of VEGF-C and VEGFR-3 correlates significantly with poor prognosis of specific types of cancer (18, 19, 21, 37–41). Marchio et al. (40) reported that tyrosine phosphorylation of VEGFR-3 is increased in Kaposi sarcoma cells treated with recombinant VEGF-C protein, and they found that activation of the VEGF-C/VEGFR-3 axis in Kaposi sarcoma cells is involved in the regulation of cellular functions, such as proliferation and migration. The VEGF-C/VEGFR-3 axis has also been found to play a role in the growth of malignant mesothelioma cells (41) and leukemic cells (21). It has become clear that the VEGF-C/VEGFR-3 axis plays an important role in promoting invasion and metastasis of human lung adenocarcinoma cells (18). It has also been reported, however, that inhibition of VEGFR-3 signaling by the soluble fusion protein VEGFR-3-immunoglobulin did not change the growth of lung cancer cells (42). These findings indicate that the effects and interactions of the VEGF-C/VEGFR-3 system in cancer biology are complex and may differ between malignancies. Previously, we reported that VEGF-C immunoreactivity is associated not only with lymphatic invasion and lymph node metastases but also with greater depth of tumor invasion in gastric cancer (16).